SUPPLEMENTARY MATERIALS: The Dynamics of Swamps in the Canonical Tensor Approximation Problem*

Martin J. Mohlenkamp†

SM1. Introduction. In these supplementary materials we present plots as described in subsections 3.3 and 3.4 for a variety of parameter values. For all plots we assume the symmetry $\boldsymbol{\phi} = \phi\mathbf{1}$ on T. Before looking at these new plots, the reader should be fluent with the key to the formatting of a single plot in Figure 3.1.

In section SM2 we consider the case $(d, z, \phi, \lambda) = (6, 1, \pi/2, 0)$ in detail, paralleling the analysis of the $(d, z, \phi, \lambda) = (6, 1, \pi/8, 0)$ case done in subsections 3.3 and 3.4. (In an earlier version of the paper, we used $(d, z, \phi, \lambda) = (6, 1, \pi/2, 0)$ in subsections 3.3 and 3.4.) We also describe experiments at producing swamps for this case.

In the remaining sections we present plots for a variety of parameter values, organized to show the effect as a single parameter varies.

- In section SM3 we fix $(z, \phi, \lambda) = (1, \pi/8, 0)$ and vary d as 30, 6, 5, 3, and 2.
- In section SM4 we fix $(d, z, \lambda) = (6, 1, 0)$ and vary ϕ as $\pi/2$, ϕ_0, $\pi/8$, and 0. The special bifurcation value ϕ_0 is derived.
- In section SM5 we fix $(d, z, \lambda) = (6, -1, 0)$ and vary ϕ as $\pi/2$, $\tilde{\phi}_0$, $\pi/8$, and the limit $\phi \to 0^+$. The special bifurcation value $\tilde{\phi}_0$ is derived, as are additional formulas for the special case $\phi \to 0^+$.
- In section SM6 we fix $(d, \phi, \lambda) = (6, \pi/8, 0)$ and vary z as 1, 1/2, 0, -1/2, and -1.
- In section SM7 we fix $(d, z, \phi) = (6, 1, \pi/8)$ and vary λ as 0, 1/100, and 1/10.
- In section SM8 we fix $(d, z, \phi) = (6, -1, \pi/8)$ and vary λ as 0, 1/100, and 1/10.

Some cases, such as $(d, z, \phi, \lambda) = (6, 1, \pi/8, 0)$, occur multiple times as we consider dependence on each variable individually. We will not comment on individual cases, but instead only make some general remarks as a single parameter varies. Each value of the tuple (d, z, ϕ, λ) gives a distinct set of plots, displayed on its own page.

- First we display the six plots using the symmetry $(\boldsymbol{\alpha}, \boldsymbol{\beta}) = (\alpha\mathbf{1}, \beta\mathbf{1})$ and axes (α, β) as described in subsection 3.3 and shown in Figures SM1, 3.2, 4.3, 4.7, and 5.1.
- Next we show the single plot using the symmetry $\alpha_2 = \cdots = \alpha_d$ and $\boldsymbol{\beta} \to \boldsymbol{\alpha}$ and axes (α_1, α_d) as described in subsection 3.4 and shown in Figures SM2 and 3.3 (but without the contour zoom). Note that when $\lambda > 0$ we can evaluate at $\boldsymbol{\beta} = \boldsymbol{\alpha}$ rather than taking the limit.
- When $z = \pm 1$ we next show the five plots using the symmetry $\alpha_2 = \cdots = \alpha_d$ and $\boldsymbol{\beta} = \boldsymbol{\phi} - \boldsymbol{\alpha}$ and axes (α_1, α_d) as described in subsection 3.4 and shown in Figures SM3, 3.4, and 4.4. When these five plots are shown, the single plot with symmetry $\boldsymbol{\beta} \to \boldsymbol{\alpha}$ is packed into the empty (upper left) spot.

*Submitted April 19, 2018; accepted in revised form May 28, 2019.
Funding: This material is based upon work supported by the National Science Foundation under Grant 1418787.
†Department of Mathematics, Ohio University, Athens OH 45701 (mohlenka@ohio.edu).

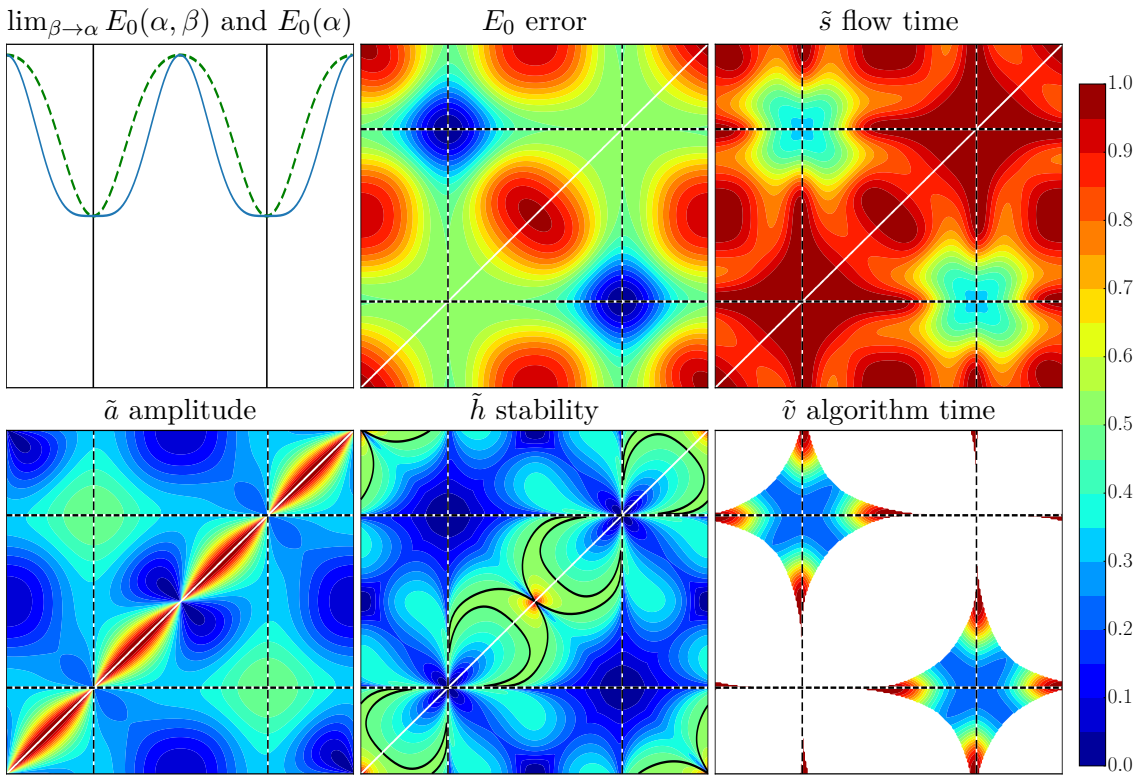

Figure SM1. *Visualization of the case* $(d, z, \phi, \lambda) = (6, 1, \pi/2, 0)$ *with symmetry* $(\boldsymbol{\alpha}, \boldsymbol{\beta}) = (\alpha\mathbf{1}, \beta\mathbf{1})$.

SM2. Detailed Analysis of the Case $(d, z, \phi, \lambda) = (6, 1, \pi/2, 0)$.

SM2.1. With Symmetry $(\boldsymbol{\alpha}, \boldsymbol{\beta}) = (\alpha\mathbf{1}, \beta\mathbf{1})$. This symmetry is described in subsection 3.3 and was used there in Figure 3.2.

In Figure SM1 we show the case $(d, z, \phi, \lambda) = (6, 1, \pi/2, 0)$. The two terms in T are orthogonal (in each direction as well) so this T is expected to be easy to recover with G_2. We observe the following:

- There is a gap between $\lim_{\beta\to\alpha} E_\lambda(\alpha, \beta)$ and $E_0(\alpha)$ except when $\alpha \in \{0, \phi/2, \phi, \phi/2 \pm \pi/2\}$. There is a notable flat spot in $\lim_{\beta\to\alpha} E_\lambda(\alpha, \beta)$ for $\alpha \in \{0, \phi\}$.
- The error E_0 has four maxima at $\{(\phi/2, \phi/2), (\phi/2, \phi/2 \pm \pi/2), (\phi/2 \pm \pi/2, \phi/2), (\phi/2 \pm \pi/2, \phi/2 \pm \pi/2)\}$ and two minima at the solutions $\{(0, \phi), (\phi, 0)\}$. There are four ordinary-looking saddles at $\{(0, \phi/2), (\phi, \phi/2), (\phi/2, 0), (\phi/2, \phi)\}$. There are also two saddle-like features on the diagonal (where E_0 is not defined) at $\{(0, 0), (\phi, \phi)\}$.
- To interpret the amplitude $\tilde{a}$ we first see that its value is around $1/2$ at the solutions $\{(0, \phi), (\phi, 0)\}$, so that is its natural size. At the two maxima of E_0 at $\{(\phi/2, \phi/2 \pm \pi/2), (\phi/2 \pm \pi/2, \phi/2)\}$ the amplitude is smaller, indicating that neither term in G_2 is effective in helping approximate T, so both are small. At the other two maxima at $\{(\phi/2, \phi/2), (\phi/2 \pm \pi/2, \phi/2 \pm \pi/2)\}$, $\tilde{a}$ has both small and large values; the large values indicate a better (but still not good) approximation can be obtained using large cancellation. The two saddle-like features on the diagonal also show this dual behavior

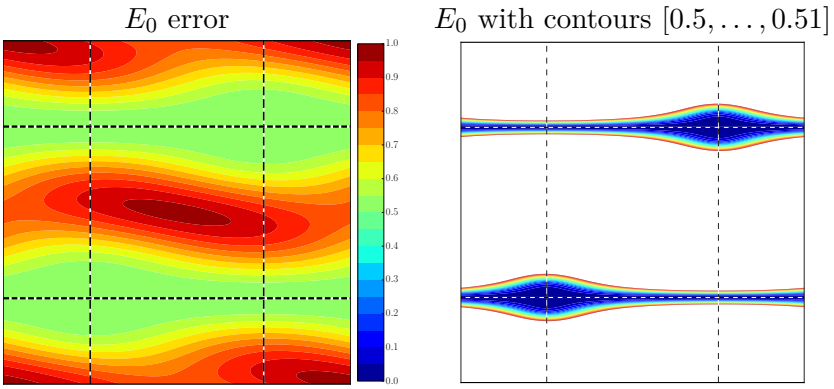

Figure SM2. *The error $E_0(\alpha_1, \alpha_d)$ in the case $(d, z, \phi, \lambda) = (6, 1, \pi/2, 0)$ with symmetry $\alpha_2 = \cdots = \alpha_d$ and $\boldsymbol{\beta} \to \boldsymbol{\alpha}$.*

of $\tilde{a}$.

- The $\tilde{h}$ stability plot shows transverse stability near the solutions $\{(0, \phi), (\phi, 0)\}$, so once in that neighborhood the flow stays in the plotting plane. At the two maxima at $\{(\phi/2, \phi/2), (\phi/2 \pm \pi/2, \phi/2 \pm \pi/2)\}$ there are both stable and unstable regions, indicating that flow from those maxima may leave the plotting plane. The two saddle-like features on the diagonal show both stable and unstable regions, with narrow spikes of instability penetrating to the features
- The flow time $\tilde{s}$ is large near the two saddle-like features on the diagonal, indicating the possibility of a transient swamp. It is relatively small near the solutions $\{(0, \phi), (\phi, 0)\}$, so there is no possibility of a terminal swamp.
- The algorithm time $\tilde{v}$ is undefined in a large region, indicating that an algorithm starting there would immediately move elsewhere, possibly breaking symmetry. There are spikes of large algorithm time extending to the two saddle-like features on the diagonal at $\{(0, 0), (\phi, \phi)\}$, again indicating the possibility of a transient swamp. It is relatively small near the solutions $\{(0, \phi), (\phi, 0)\}$, again indicating there is no possibility of a terminal swamp.

SM2.2. With Symmetry $\alpha_2 = \cdots = \alpha_d$ and $\boldsymbol{\beta} \to \boldsymbol{\alpha}$. This symmetry is described in subsection 3.4 and was used there in Figure 3.3.

Figure SM2 gives $E_0(\alpha_1, \alpha_d)$ for $(d, z, \phi, \lambda) = (6, 1, \pi/2, 0)$. We observe that the minima occur at $\{(0, 0), (\phi, \phi)\}$ and thus the flow under this symmetry should move back to the full symmetry $\boldsymbol{\alpha} = \alpha \mathbf{1}$ and exit at the saddle-like features at $\{(0, 0), (\phi, \phi)\}$ observed in subsection 3.3; we must consider this observation as tentative, since the flow could leave the current symmetry before getting near the minimum within it. Note that the quantity $\lim_{\beta \to \alpha} E_0(\alpha, \beta)$ in Figure SM1 appears on the diagonal in Figure SM2.

SM2.3. With Symmetry $\alpha_2 = \cdots = \alpha_d$ and $\boldsymbol{\beta} = \phi - \boldsymbol{\alpha}$. This symmetry is described insubsection 3.4 and was used there in Figure 3.4.

Figure SM3 gives the five available plots for $(d, z, \phi, \lambda) = (6, 1, \pi/2, 0)$. We observe the following:

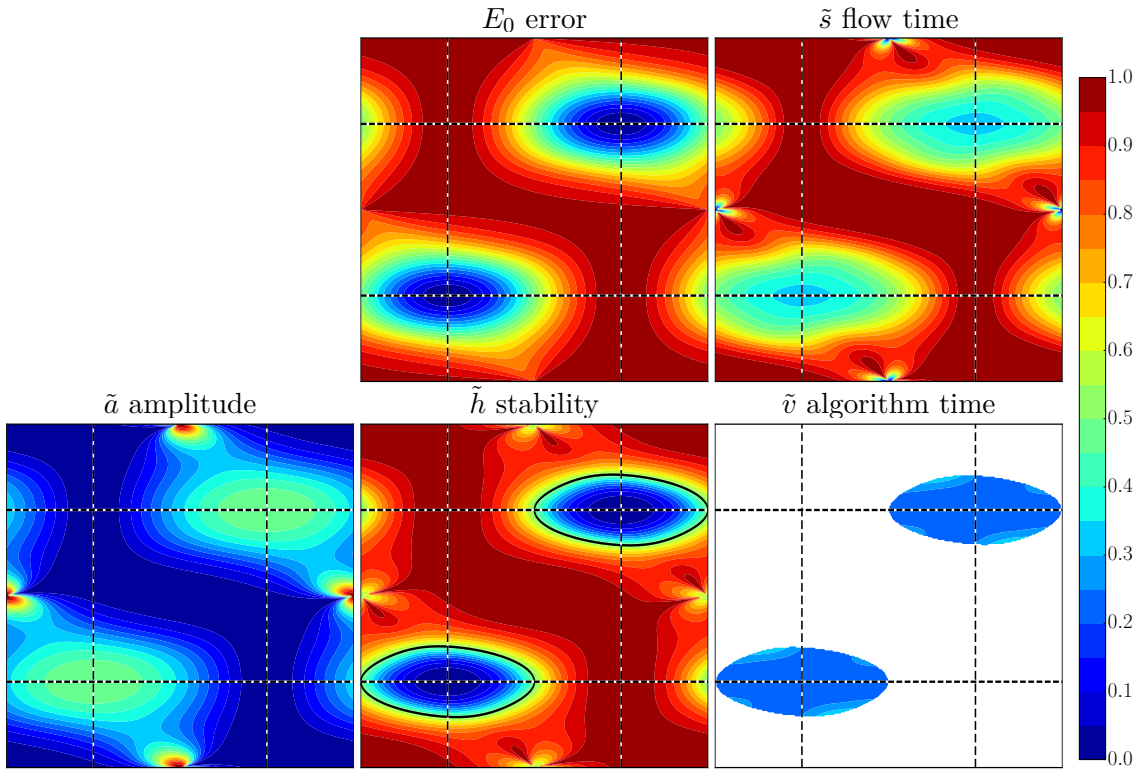

Figure SM3. *Visualization of the case* $(d, z, \phi, \lambda) = (6, 1, \pi/2, 0)$ *under the constraints* $\alpha_2 = \cdots = \alpha_d$ *and* $\boldsymbol{\beta} = \phi - \boldsymbol{\alpha}$*, with horizontal axis* α_1 *and vertical axis* α_d*.*

- The error E_0 has two minima at the solutions $\{(0,0),(\phi,\phi)\}$. Away from the minima it is large without distinct features.
- The amplitude $\tilde{a}$ is small in the region where the error is large. The amplitude $\tilde{a}$ is large near $(\alpha_1, \alpha_d) = (\phi/2, \phi/2 \pm \pi/2)$ and $(\alpha_1, \alpha_d) = (\phi/2 \pm \pi/2, \phi/2)$, which correspond respectively to $(\beta_1, \beta_d) = (\phi/2, \phi/2 \mp \pi/2)$ and $(\beta_1, \beta_d) = (\phi/2 \mp \pi/2, \phi/2)$. Since the error and other quantities are π-periodic, these points correspond to the diagonal $\boldsymbol{\alpha} = \boldsymbol{\beta}$.
- The $\tilde{h}$ stability plot shows transverse stability near the solutions $\{(0,0),(\phi,\phi)\}$, so once in that neighborhood the flow stays in the plotting plane. Away from the solutions the flow is unstable.
- The flow time $\tilde{s}$ is large when the error is large, as expected. It is relatively small near the solutions $\{(0,0),(\phi,\phi)\}$, so there is no possibility of a terminal swamp.
- The algorithm time $\tilde{v}$ is small near the solutions $\{(0,0),(\phi,\phi)\}$, which indicates no possibility of a terminal swamp. It is undefined elsewhere, which indicates no transient swamp in this symmetry.

Note that the diagonal $\alpha_1 = \alpha_d$ in Figure SM3 is the anti-diagonal $\beta = \phi - \alpha$ in Figure SM1.

SM2.4. Swamp Experiments. Figure SM1 showed very flat saddle-like features at $(0,0)$ and (ϕ,ϕ) that could produce transient swamps. Starting at either $(\boldsymbol{\alpha}, \boldsymbol{\beta}) = ((\phi/4)\mathbf{1}, (-\phi/4)\mathbf{1})$

or $(\boldsymbol{\alpha}, \boldsymbol{\beta}) = ((\phi/2)\mathbf{1}, (\phi/4)\mathbf{1})$ results in the numerical breakdown of ALS. Reducing ϕ slightly, we observe two different behaviors.

- Starting at $(\boldsymbol{\alpha}, \boldsymbol{\beta}) = ((\phi/4)\mathbf{1}, (-\phi/4)\mathbf{1})$, setting $\phi = (15/32)\pi$ results in a transient swamp of length 785 and setting $\phi = (7/16)\pi$ results in one of length 21. The flow stays in the symmetric set $(\boldsymbol{\alpha}, \boldsymbol{\beta}) = (\alpha\mathbf{1}, \beta\mathbf{1})$, first passing near the saddle-like essential saddle near $(\alpha, \beta) = (0, 0)$ and then proceeding down a valley to $(\alpha, \beta) = (\phi, 0)$. The valley, with cusp-like level curves, is visible in Figure SM1. Since $\phi > \phi_0 =$ (SM4.3), the best G_1 approximation is near either $\alpha = 0$ or $\alpha = \phi$ (see Theorem SM4.1). Thus we have a situation where both terms in G_2 go to the same (local) best G_1 and then escape through a transient swamp, as we did in subsection 4.2.
- Starting at $(\boldsymbol{\alpha}, \boldsymbol{\beta}) = ((\phi/2)\mathbf{1}, (\phi/4)\mathbf{1})$, setting $\phi = (15/32)\pi$ results in a transient swamp of length 3010 and $\phi = (7/16)\pi$ results in one of length 75. In this case the $\boldsymbol{\beta}$ term approximates the G_1 solution at 0 while the $\boldsymbol{\alpha}$ term initially contributes little. The $\boldsymbol{\alpha}$ term breaks symmetry and α_1 decreases past $\phi/2 - \pi/2$ (similar to subsection 4.4). Once it returns to symmetry, convergence is rapid.

We have not seen such swamps mentioned in the literature and suspect they do not occur in practice.

SM3. Varying d with $(z, \phi, \lambda) = (1, \pi/8, 0)$. The following pages show d values 30, 6, 5, 3, and 2.

- At large $d = 30$, the interesting features are shrunk to a smaller part of the plot.
- There is no qualitative difference between even $d = 6$ and odd $d = 5$.
- For $d = 2$, which is a matrix approximation rather than a tensor approximation, the point solutions $(\alpha, \beta) = (0, \phi)$ and $(\alpha, \beta) = (\phi, 0)$ become a manifold of solutions.

SM3.1. $(d, z, \phi, \lambda) = (30, 1, \pi/8, 0)$.

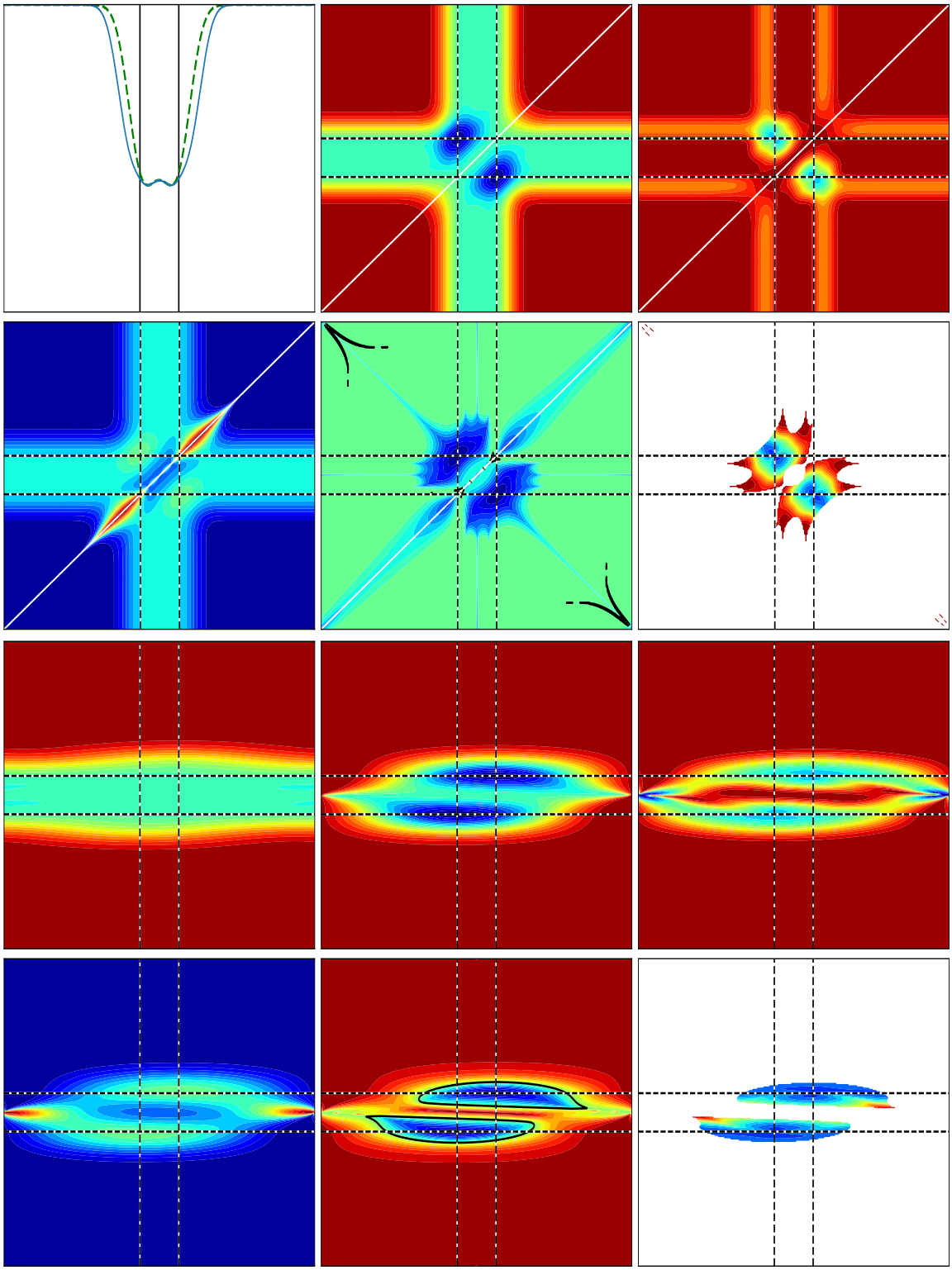

SM3.2. $(d, z, \phi, \lambda) = (6, 1, \pi/8, 0)$.

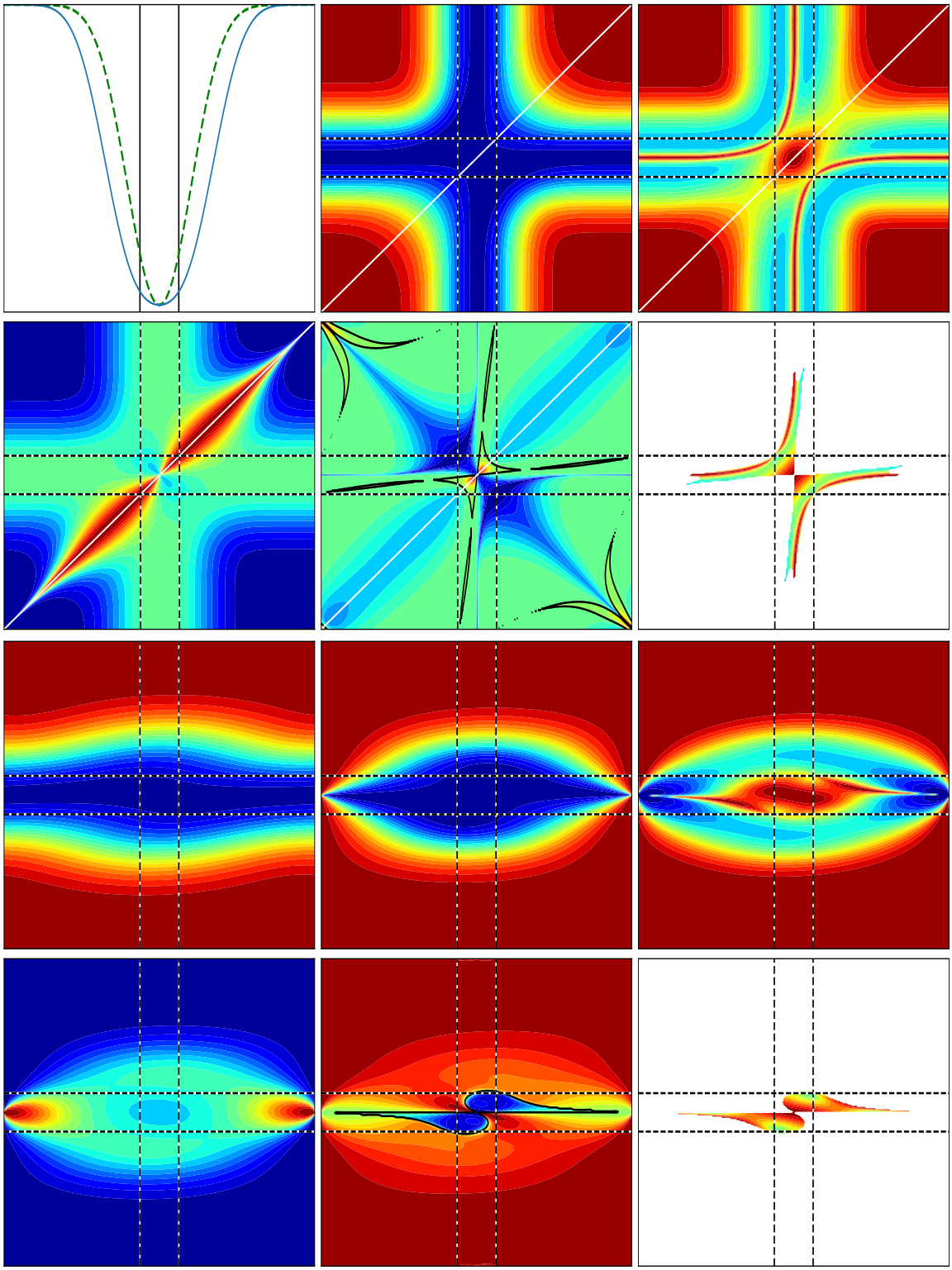

SM3.3. $(d, z, \phi, \lambda) = (5, 1, \pi/8, 0)$.

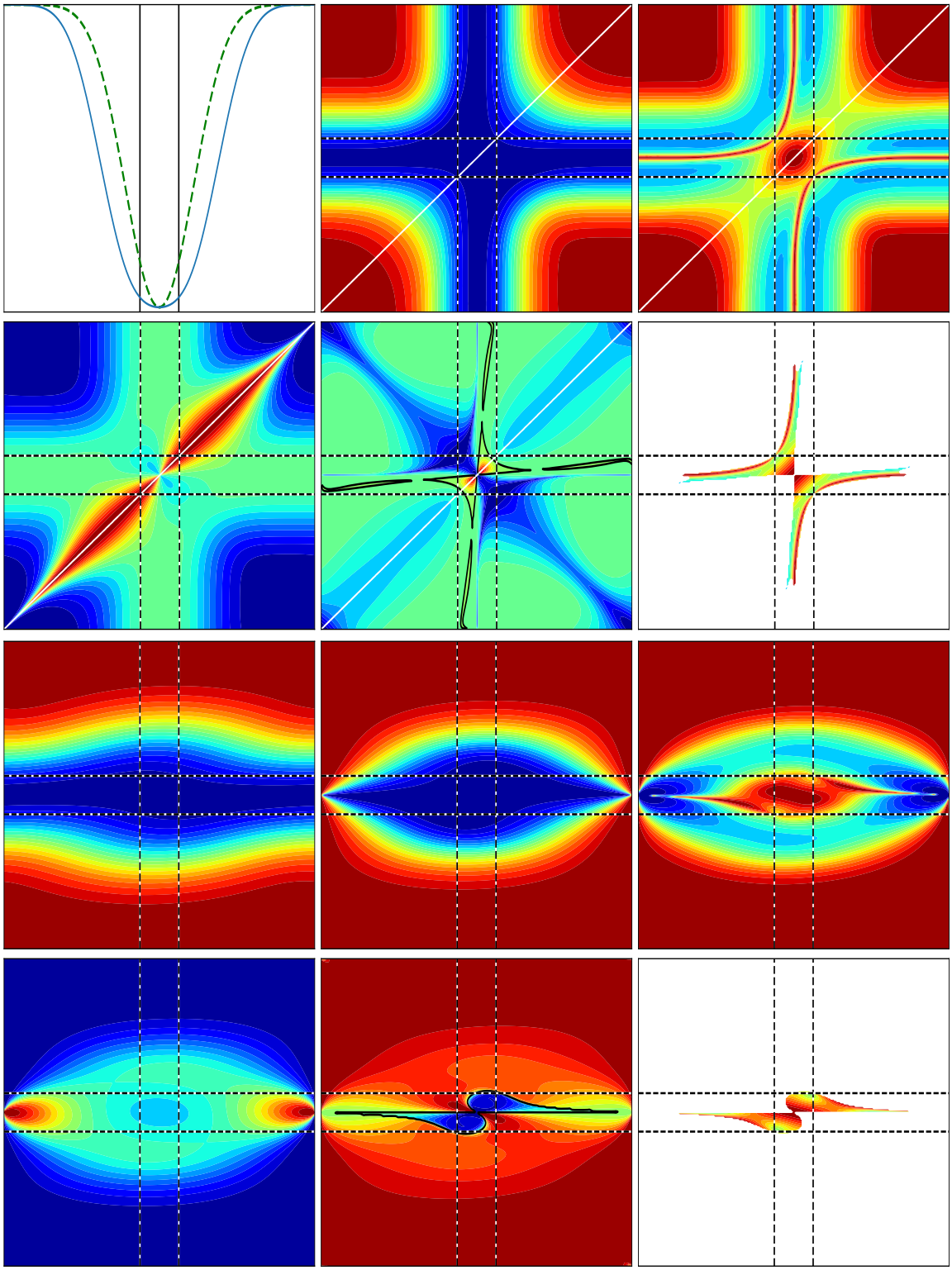

SM3.4. $(d, z, \phi, \lambda) = (3, 1, \pi/8, 0)$.

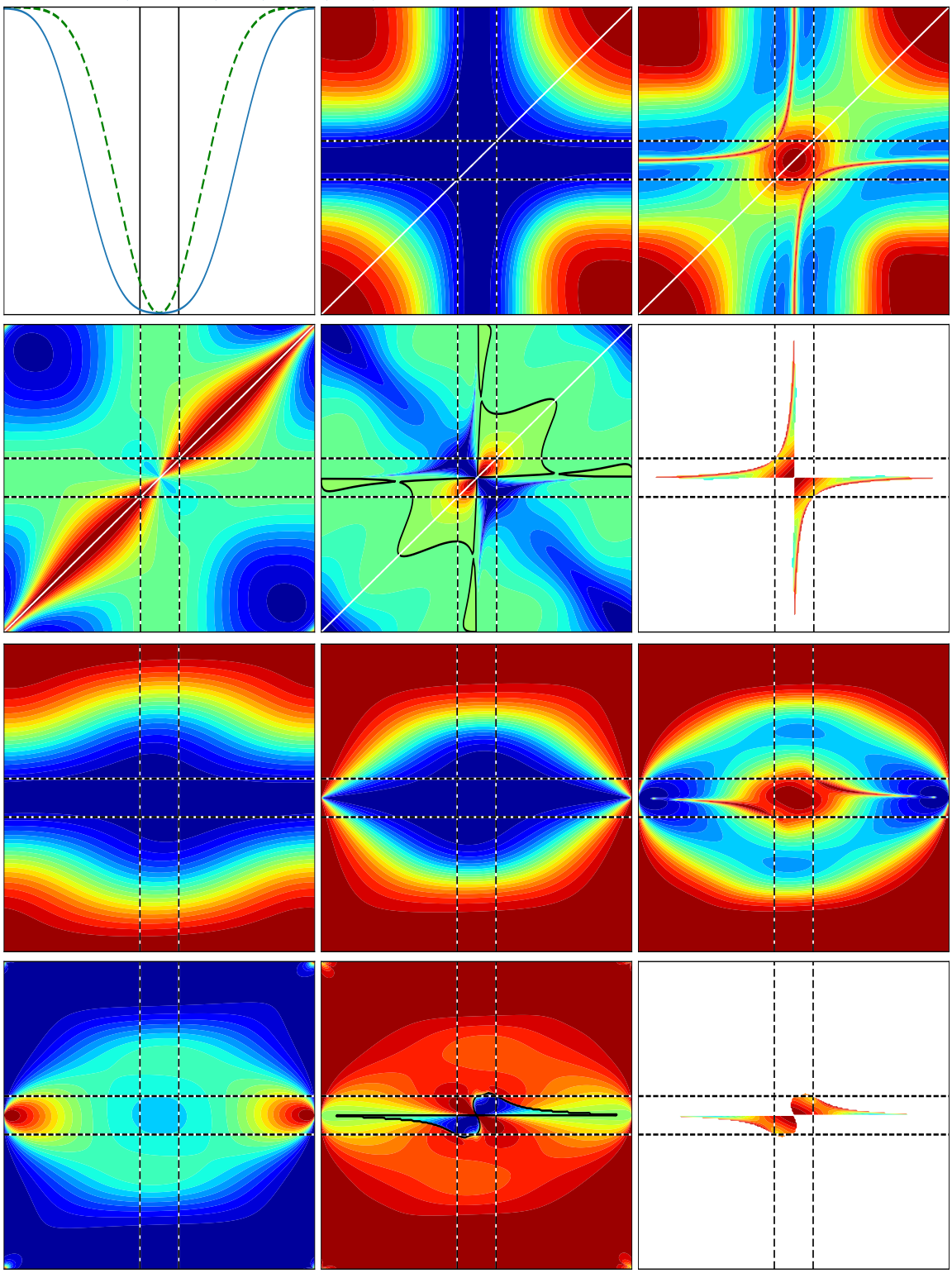

SM3.5. $(d, z, \phi, \lambda) = (2, 1, \pi/8, 0)$.

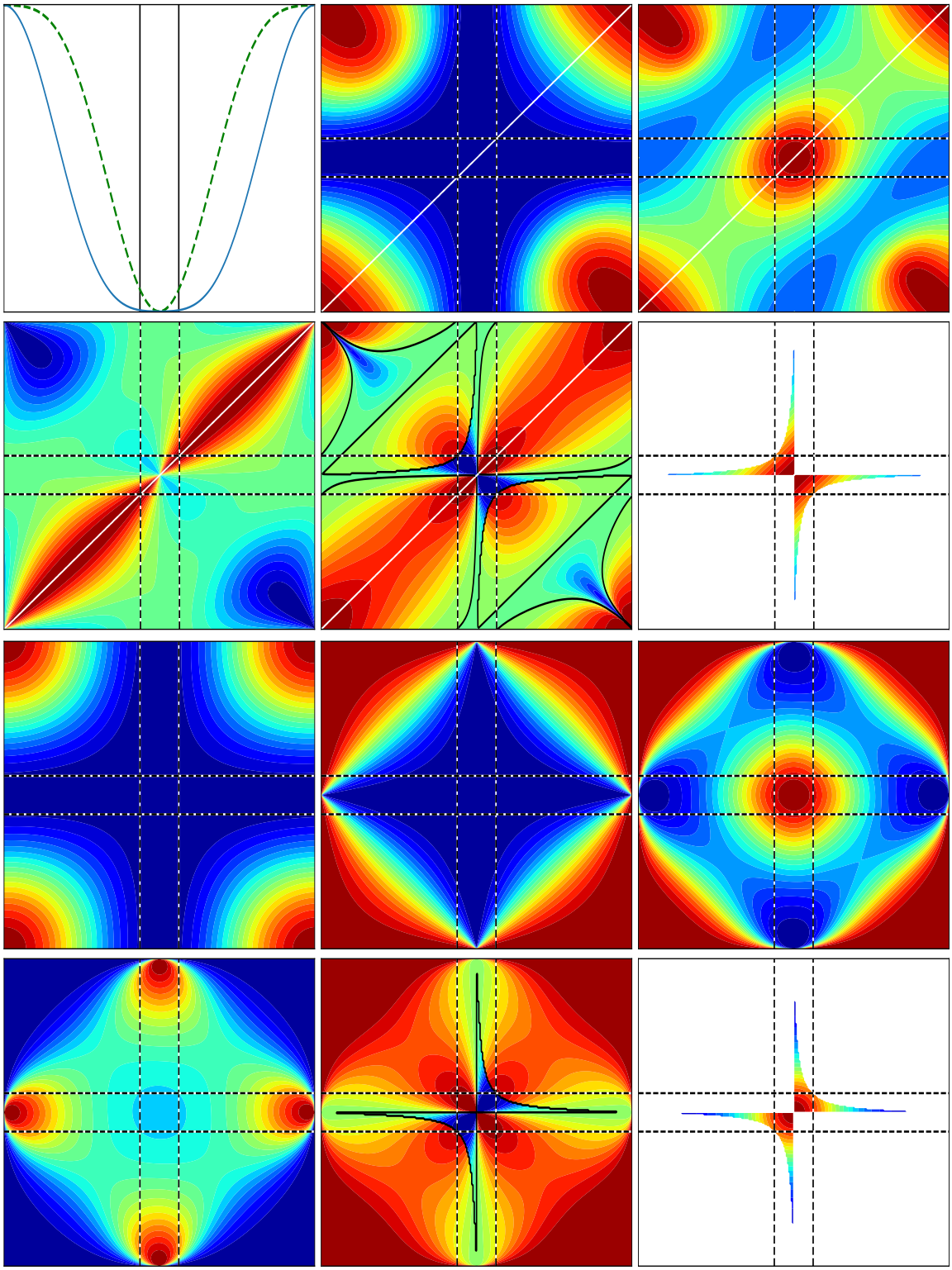

SM4. Varying ϕ with $(d, z, \lambda) = (6, 1, 0)$. The following pages show ϕ values $\pi/2$, $\phi_0 =$ (SM4.3), $\pi/8$, and 0.

- There is a qualitative bifurcation in behavior at $\phi = \phi_0$ when valleys merge.
- At $\phi = 0$, the rank-2 target T collapses to rank 1. If either $\alpha = 0$ or $\beta = 0$ then $E_0(\alpha, \beta) = 0$.

The special value ϕ_0 was determined in [SM1, subsection 4.3] as a bifurcation point for G_1, where $E_0(\phi/2)$ switches from being a minimum to a maximum. That it is relevant for the G_2 error is shown by considering $\lim_{\beta\to\alpha} E_0(\alpha, \beta)$. In Lemmas A.2 and A.3 we considered the general case where $\boldsymbol{\beta} = \boldsymbol{\alpha} + \epsilon\mathbf{v}$ with $\|\mathbf{v}\| = 1$. Inserting our assumptions $\boldsymbol{\phi} = \phi\mathbf{1}$, $\boldsymbol{\alpha} = \alpha\mathbf{1}$, and $\boldsymbol{\beta} = \beta\mathbf{1}$, we obtain

$$\text{(SM4.1)} \qquad \text{(A.23)} \mapsto \qquad \lim_{\beta\to\alpha} E_0(\alpha, \beta) = 1 - \left(n^2(\boldsymbol{\alpha}) + d n_j^2(\boldsymbol{\alpha})\right) \quad \text{and}$$

$$\text{(SM4.2)} \qquad \text{(A.26)} \mapsto \qquad \lim_{\beta\to\alpha} \begin{bmatrix} a \\ b \end{bmatrix} = \frac{n(\boldsymbol{\alpha})}{2} \begin{bmatrix} 1 \\ 1 \end{bmatrix} + \frac{1}{2} \left(\lim_{\beta\to\alpha} \frac{n_j(\boldsymbol{\beta})}{-p_j(\boldsymbol{\alpha} - \boldsymbol{\beta})} \right) \begin{bmatrix} 1 \\ -1 \end{bmatrix},$$

which diverges except possibly when $n_j(\boldsymbol{\alpha}) = 0$.

Theorem SM4.1. *If $z = 1$ and $\lambda = 0$, then the limiting error function (SM4.1) has a bifurcation at*

$$\text{(SM4.3)} \qquad \phi_0 = 2 \arcsin\left(d^{-1/2}\right) = 2 \arctan\left((d-1)^{-1/2}\right),$$

with a local minimum at $\phi/2$ when $0 < \phi < \phi_0$ and a local maximum when $\phi_0 < \phi \leq \pi/2$.

Proof. We compute

$$\text{(SM4.4)} \qquad \frac{\mathrm{d}^2}{\mathrm{d}\alpha^2}\left(1 - \left(n^2(\boldsymbol{\alpha}) + d n_j^2(\boldsymbol{\alpha})\right)\right)_{z=1}\Big|_{\alpha=\phi/2} = \frac{4d(d-1)\cos^{2d-4}(\phi/2)\sin^2(\phi/2)(1 - d\sin^2(\phi/2))}{1 + \cos^d(\phi)},$$

which is zero at $\phi_0 =$ (SM4.3). Checking the signs of (SM4.4) on each side of the bifurcation shows that larger ϕ yield maxima and smaller ϕ yield minima. ∎

SM4.1. $(d, z, \phi, \lambda) = (6, 1, \pi/2, 0)$.

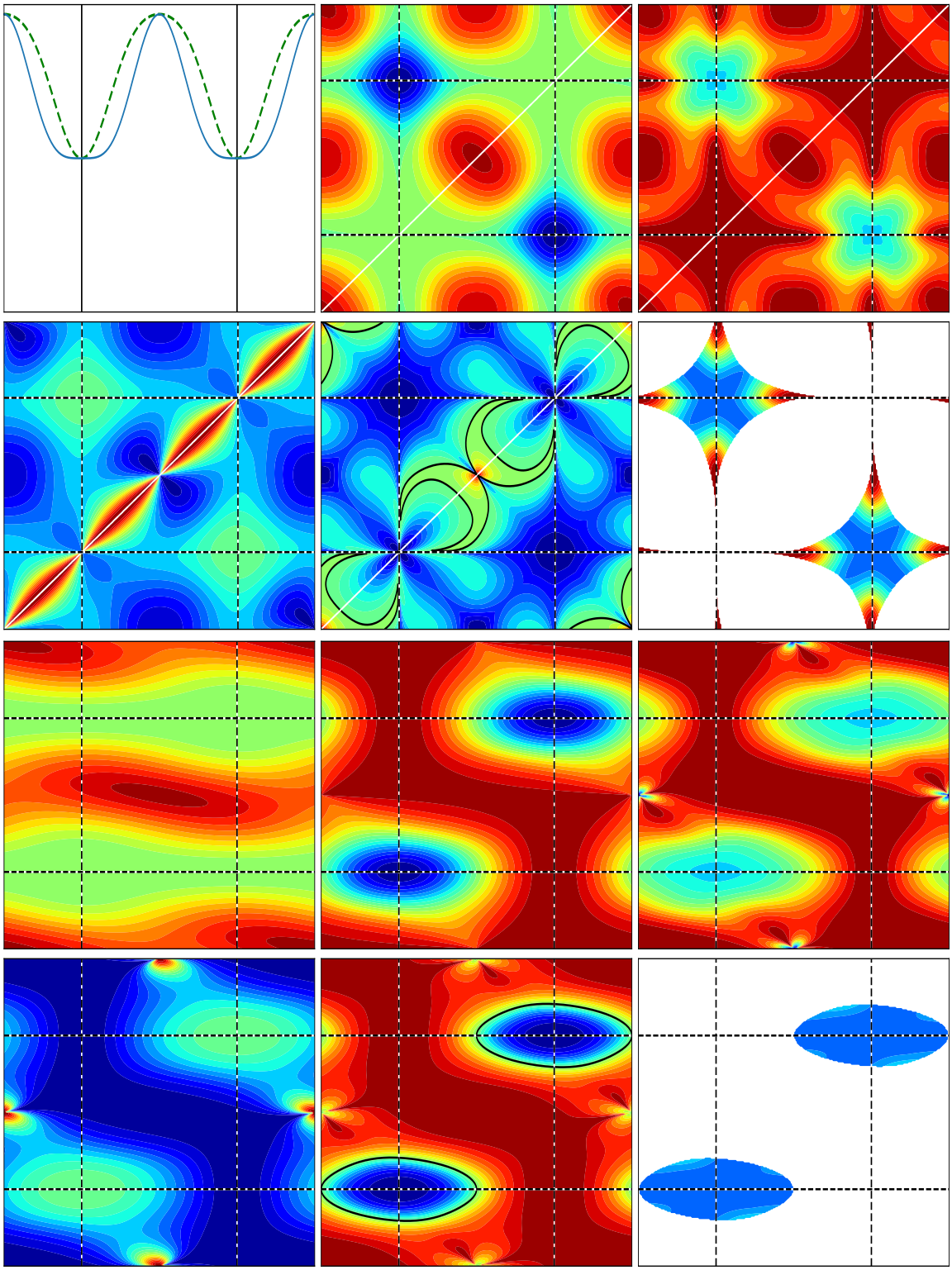

SM4.2. $(d, z, \phi, \lambda) = (6, 1, \phi_0, 0)$.

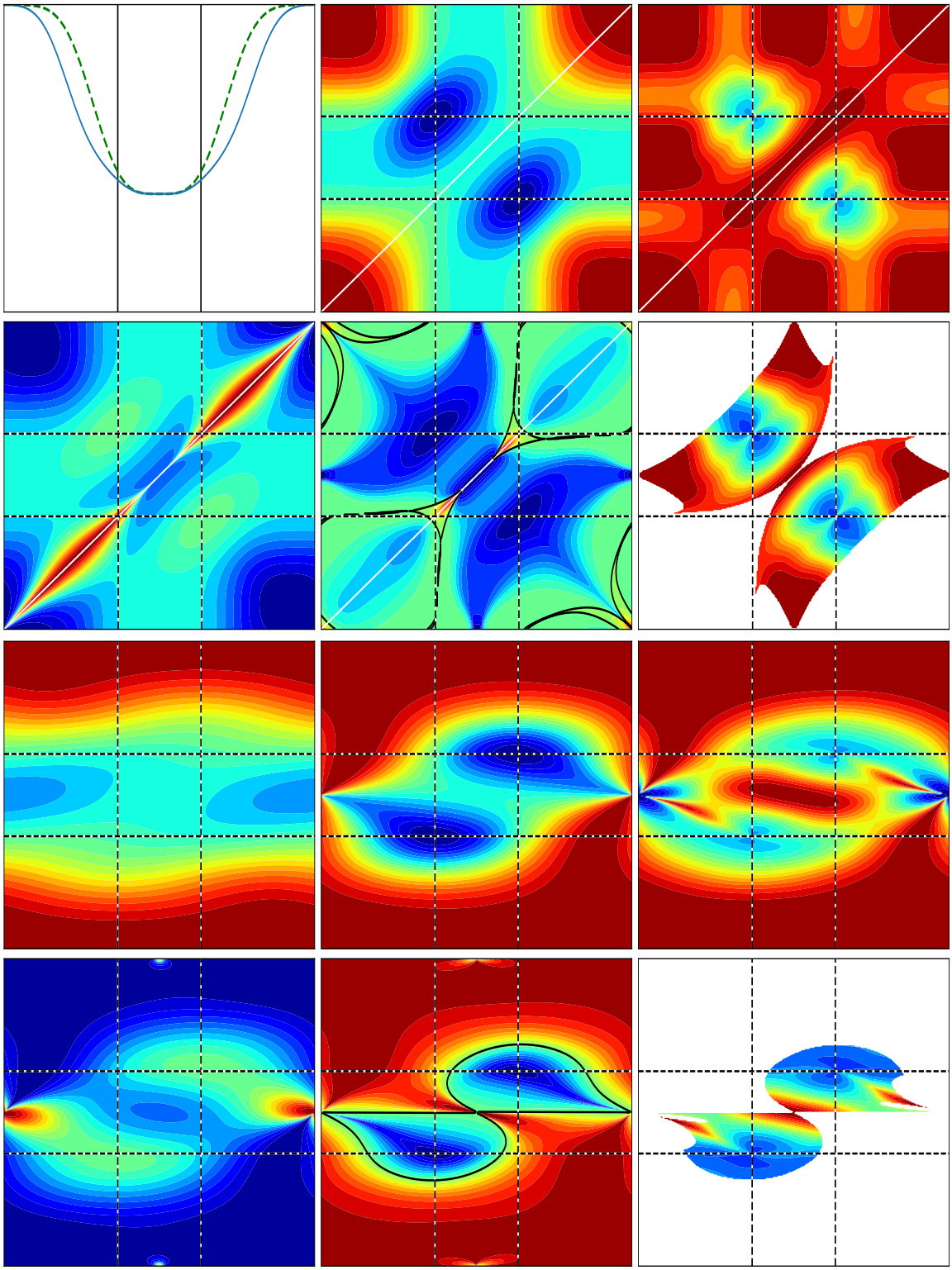

SM4.3. $(d, z, \phi, \lambda) = (6, 1, \pi/8, 0)$.

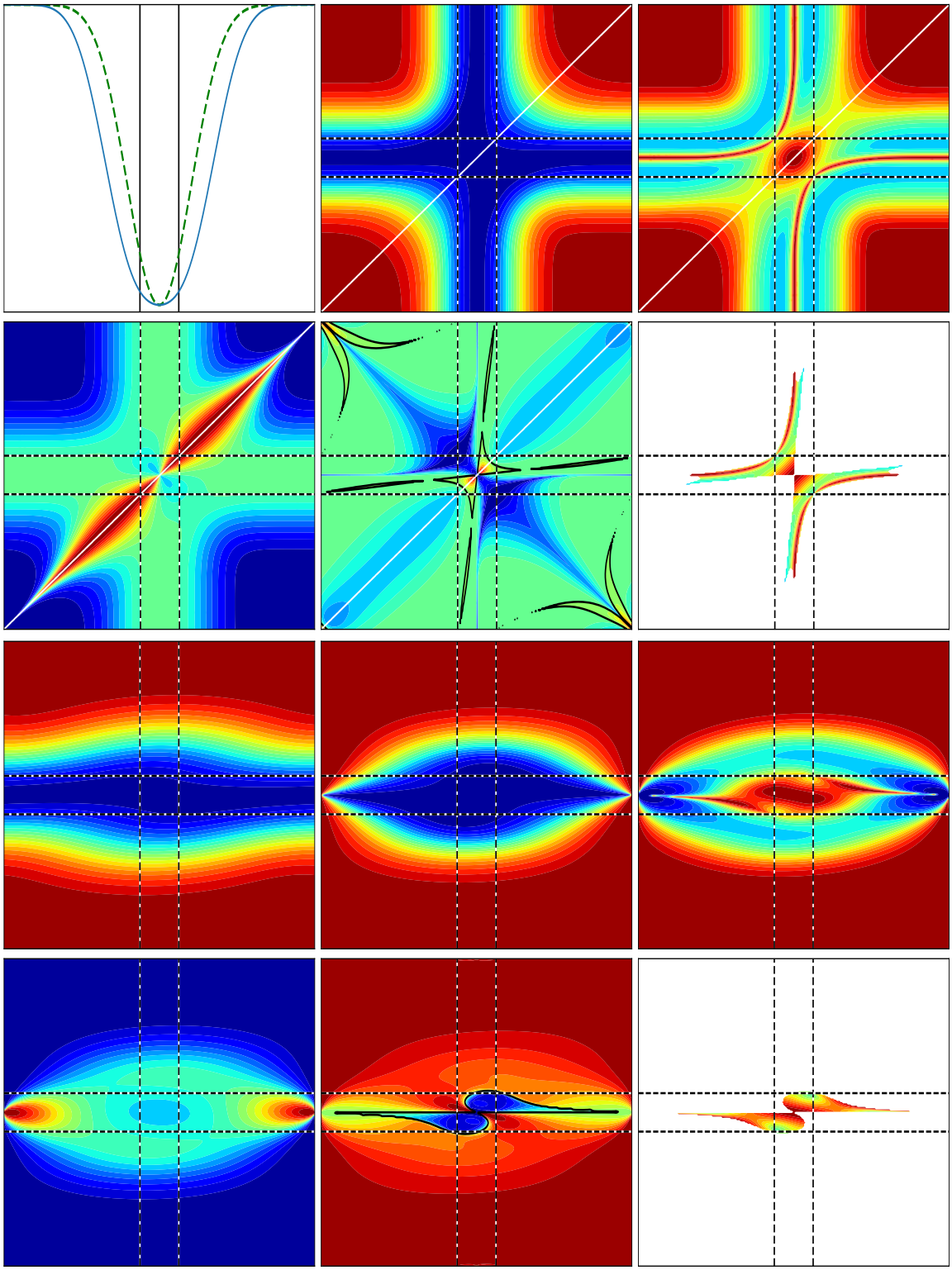

SM4.4. $(d, z, \phi, \lambda) = (6, 1, 0, 0)$.

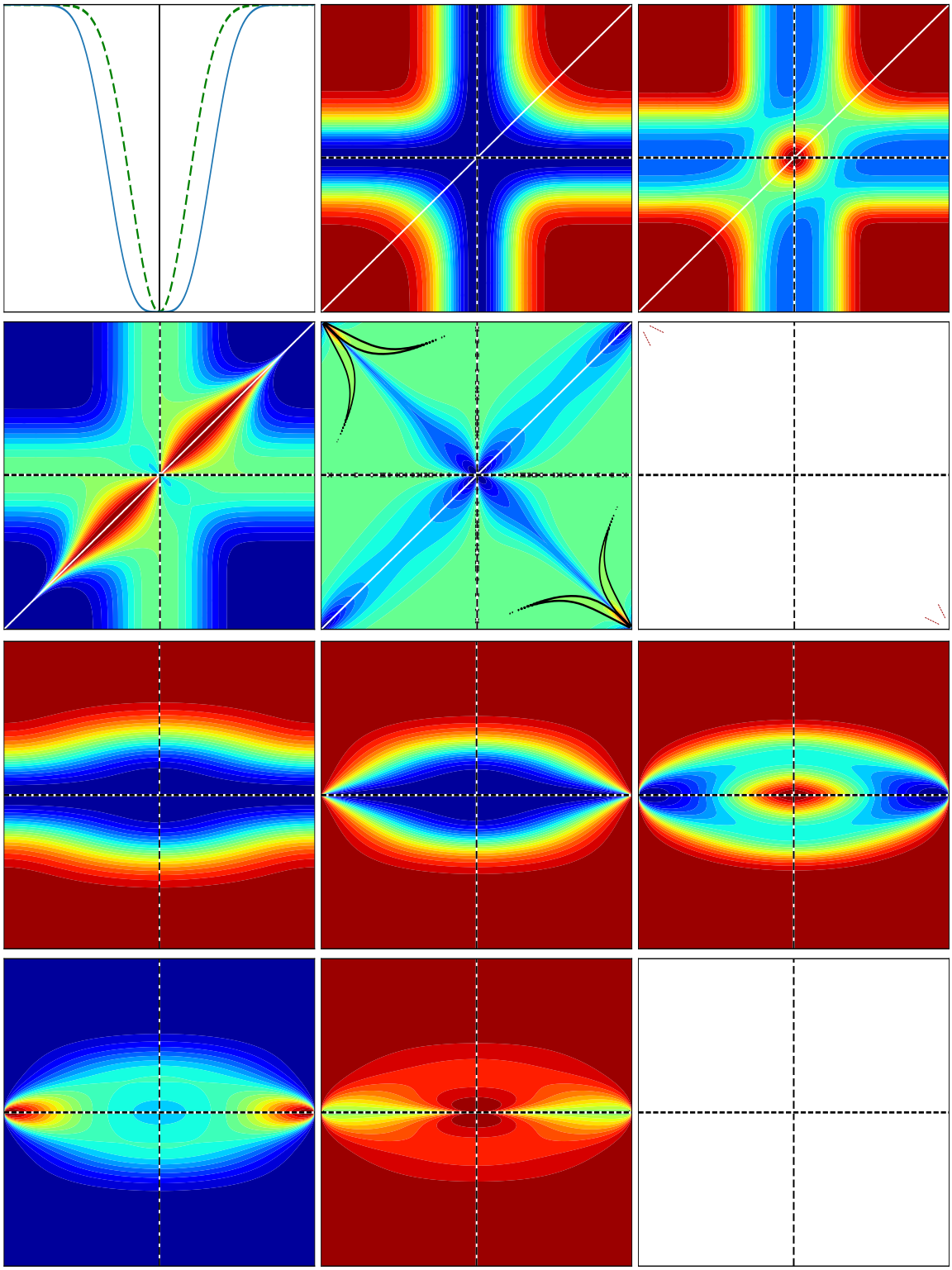

SM5. Varying ϕ with $(d, z, \lambda) = (6, -1, 0)$. The following pages show ϕ values $\pi/2$, $\tilde{\phi}_0 =$ (SM5.1), $\pi/8$, and the limit $\phi \to 0^+$.

- There is a qualitative bifurcation in behavior at $\phi = \tilde{\phi}_0$ when the central maximum becomes a saddle.
- The $\phi \to 0^+$ plot looks similar to the $\phi = \pi/8$ case, but the two solutions have merged into the diagonal and become an infimum.

The special value $\tilde{\phi}_0$ does not occur in the G_1 case but can be found through the same process as in Theorem SM4.1

Theorem SM5.1. *If $z = -1$ and $\lambda = 0$, then the limiting error function (SM4.1) has a bifurcation at*

$$\tilde{\phi}_0 = 2 \arcsin\left(\sqrt{\frac{2}{d}}\right) = 2 \arctan\left(\sqrt{\frac{2}{d-2}}\right), \tag{SM5.1}$$

with a local minimum at $\phi/2$ when $0 < \phi < \tilde{\phi}_0$ and a local maximum when $\tilde{\phi}_0 < \phi \leq \pi/2$.

Proof. We compute

$$\frac{\mathrm{d}^2}{\mathrm{d}\alpha^2}\Big(1 - \Big(n^2(\boldsymbol{\alpha}) + d n_j^2(\boldsymbol{\alpha})\Big)\Big)_{z=-11}\Big|_{\alpha=\phi/2} = \frac{4d(d-1)\cos^{2d-4}(\phi/2)\sin^2(\phi/2)(2 - d\sin^2(\phi/2))}{1 - \cos^d(\phi)}, \tag{SM5.2}$$

which is zero at $\tilde{\phi}_0 =$ (SM5.1). Checking the signs of (SM5.2) on each side of the bifurcation shows that larger ϕ yield maxima and smaller ϕ yield minima. ∎

Enforcing the symmetry $\boldsymbol{\phi} = \phi\mathbf{1}$ and then taking $\phi \to 0^+$, the rank-2 target T jumps to rank d and can be written as

$$L = \frac{-1}{\sqrt{d}} \sum_{m=1}^{d} \left(\bigotimes_{i=1, i\neq m}^{d} \begin{bmatrix} 1 \\ 0 \end{bmatrix} \right) \otimes_m \begin{bmatrix} 0 \\ 1 \end{bmatrix}, \tag{SM5.3}$$

where $\otimes_m$ indicates inserting the following term in direction m in the tensor product. The definitions of $n(\boldsymbol{\alpha})$, $n_j(\boldsymbol{\alpha})$, and $n_{jk}(\boldsymbol{\alpha})$ in Appendix A.1 change to

$$n(\boldsymbol{\alpha}) = \left\langle \bigotimes_{i=1}^{d} \mathbf{u}(\alpha_i), L \right\rangle = \frac{-1}{\sqrt{d}} \sum_{m=1}^{d} \left(\sin(\alpha_m) \prod_{i=1, \neq m}^{d} \cos(\alpha_i) \right) = \frac{1}{\sqrt{d}} \sum_{m=1}^{d} p_m(\boldsymbol{\alpha}), \tag{SM5.4}$$

$$n_j(\boldsymbol{\alpha}) = \frac{1}{\sqrt{d}} \sum_{m=1}^{d} p_{mj}(\boldsymbol{\alpha}), \quad \text{and} \tag{SM5.5}$$

$$n_{jk}(\boldsymbol{\alpha}) = \frac{-1}{\sqrt{d}} \left(p_j(\boldsymbol{\alpha}) + p_k(\boldsymbol{\alpha}) + \sum_{m=1, \neq j, \neq k}^{d} \sin(\alpha_m)\sin(\alpha_j)\sin(\alpha_k) \left(\prod_{i=1, \neq m, \neq j, \neq k}^{d} \cos(\alpha_i) \right) \right). \tag{SM5.6}$$

Formulas in Appendix A expressed in terms of these quantities then still hold.

SM5.1. $(d, z, \phi, \lambda) = (6, -1, \pi/2, 0)$.

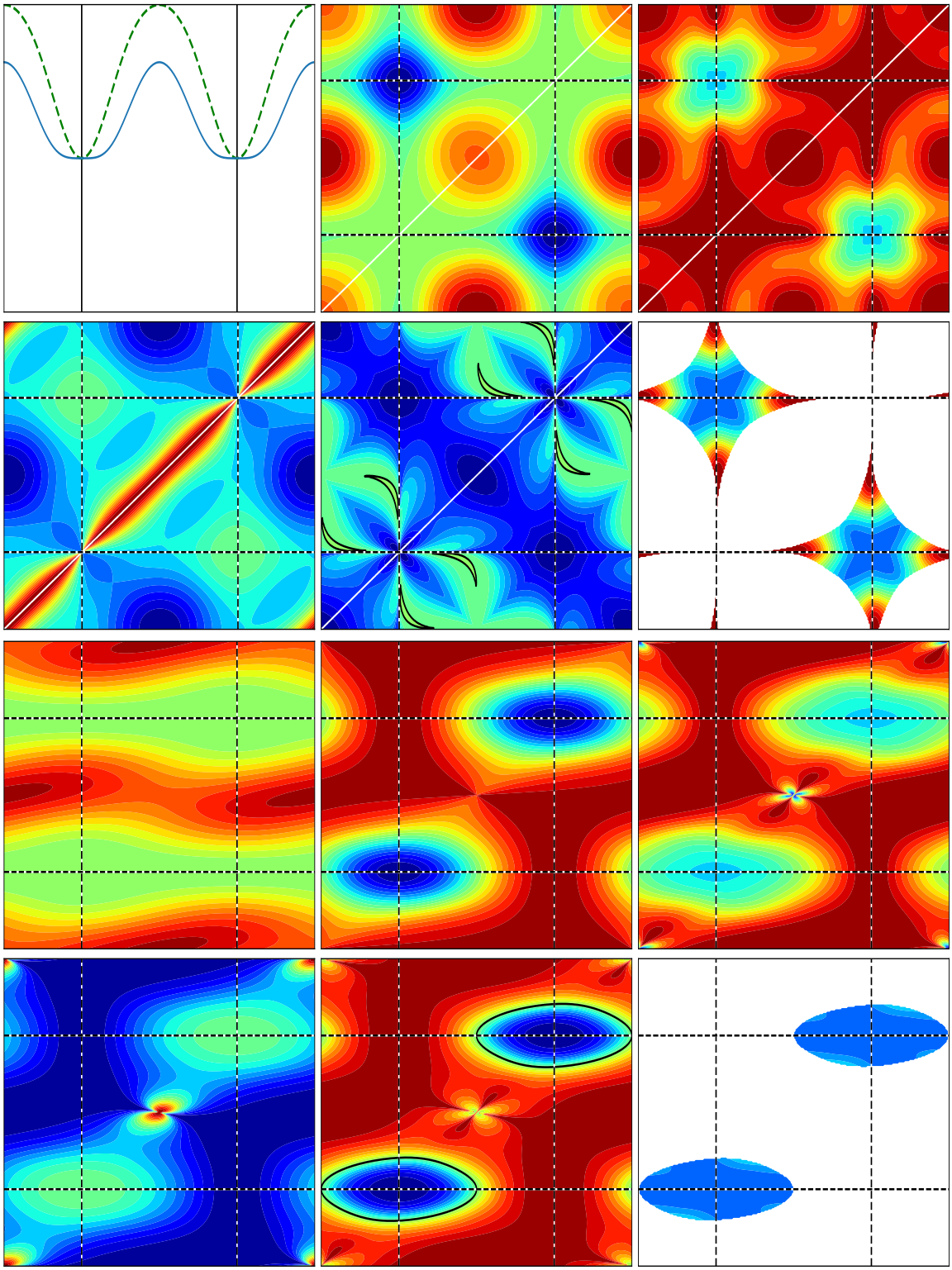

SM5.2. $(d, z, \phi, \lambda) = (6, -1, \tilde{\phi}_0, 0)$.

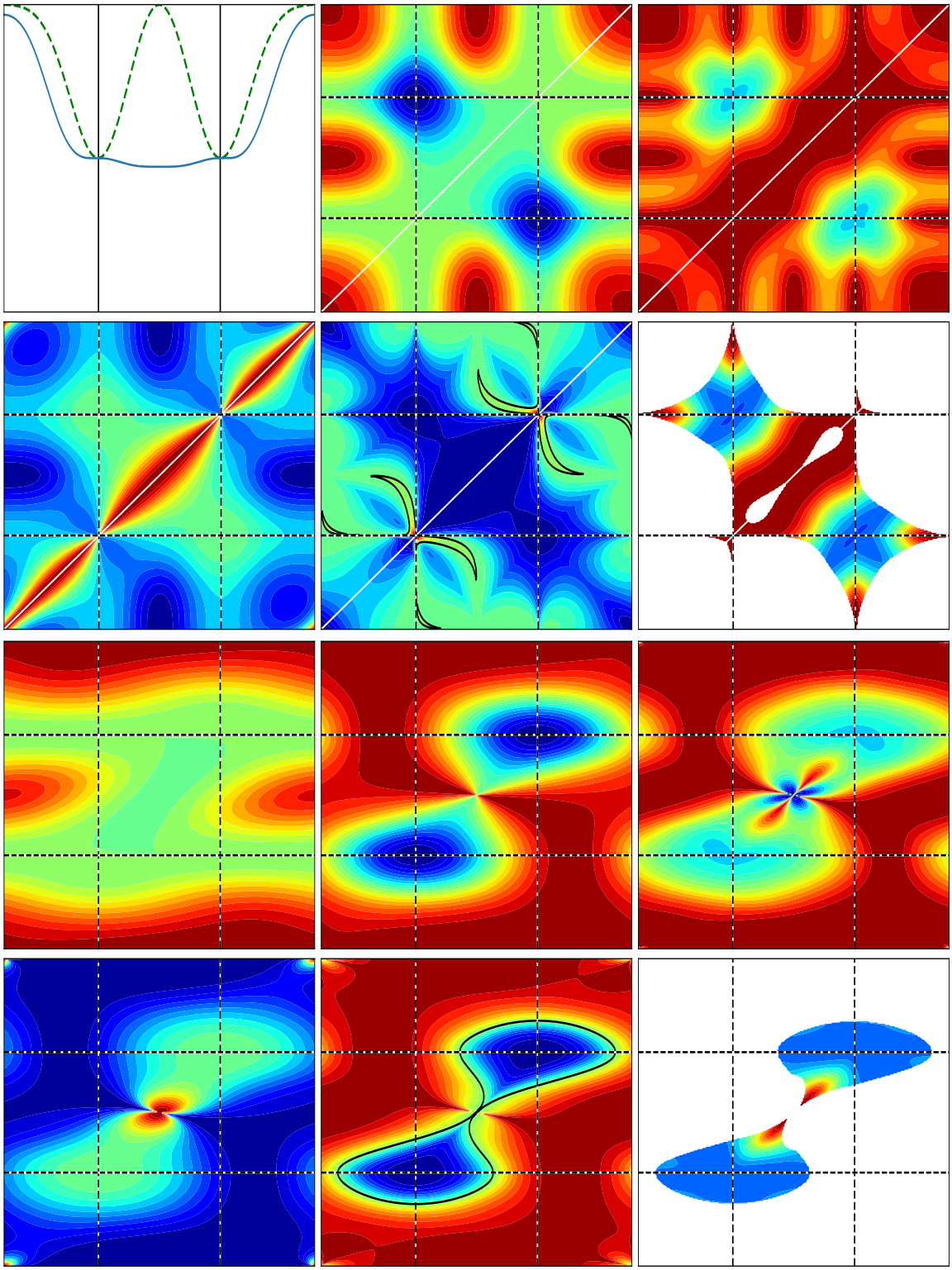

SM5.3. $(d, z, \phi, \lambda) = (6, -1, \pi/8, 0)$.

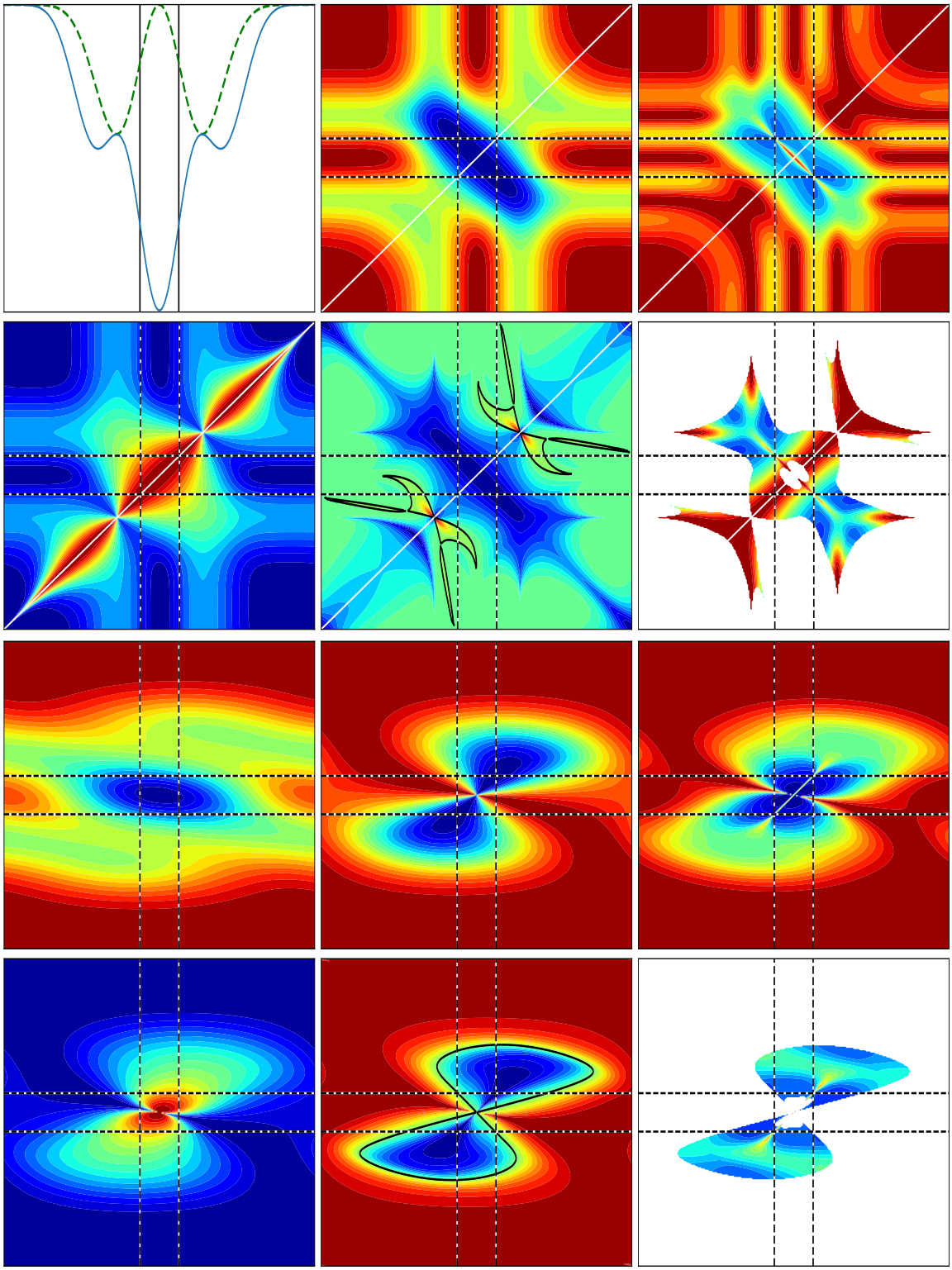

SM5.4. $(d, z, \phi, \lambda) = (6, -1, \to 0^+, 0)$.

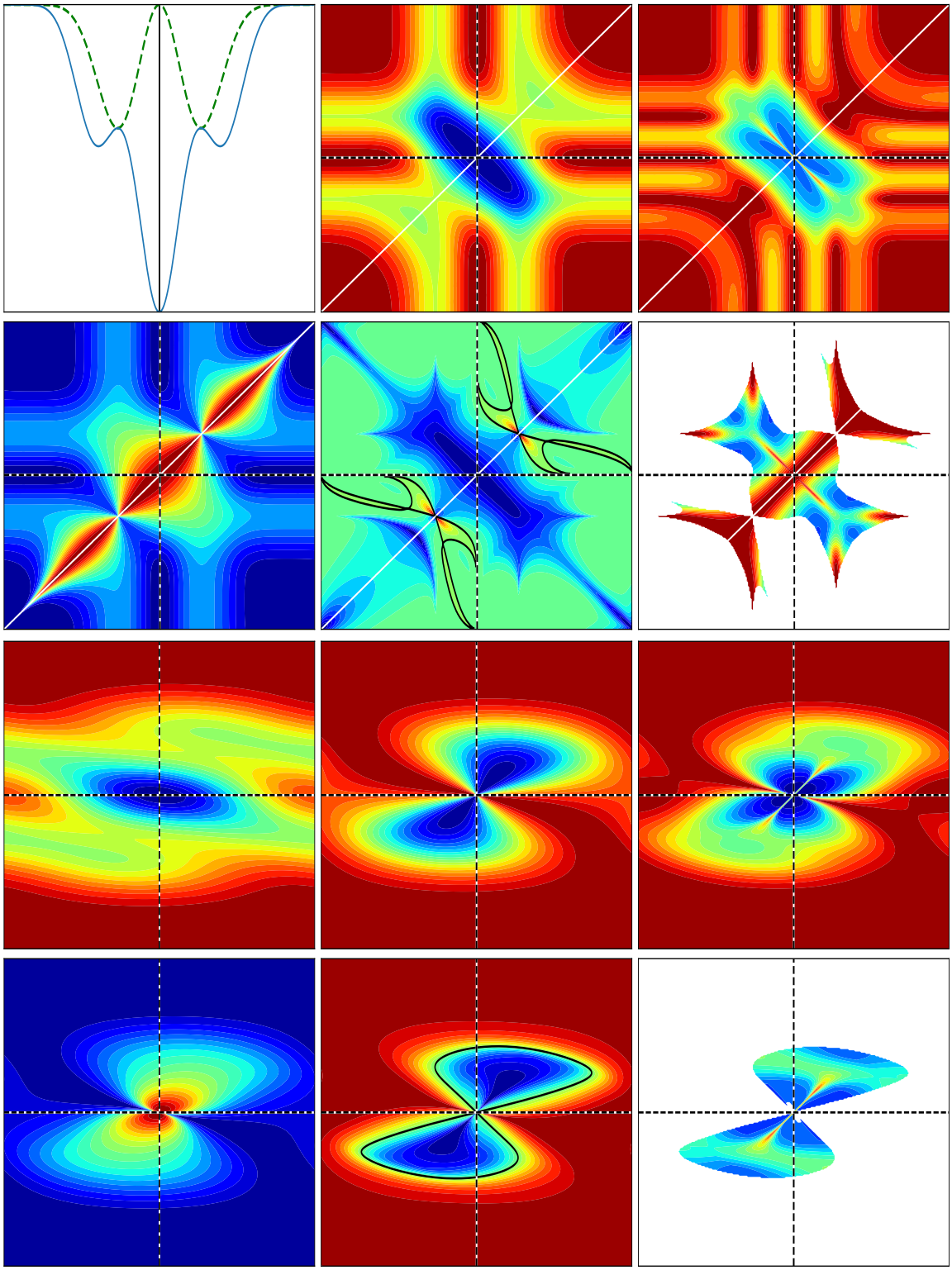

SM6. Varying z with $(d, \phi, \lambda) = (6, \pi/8, 0)$. The following pages show z values 1, 1/2, 0, -1/2, and -1.

- When $|z| < 1$, the error landscape is skewed toward the larger term.
- At $z = 0$, the rank-2 target T collapses to rank 1. If either $\alpha = 0$ or $\beta = 0$ then $E_0(\alpha, \beta) = 0$.
- There is a qualitative difference between $0 < z$ and $z < 0$ in the orientation of the valleys.

SM6.1. $(d, z, \phi, \lambda) = (6, 1, \pi/8, 0)$.

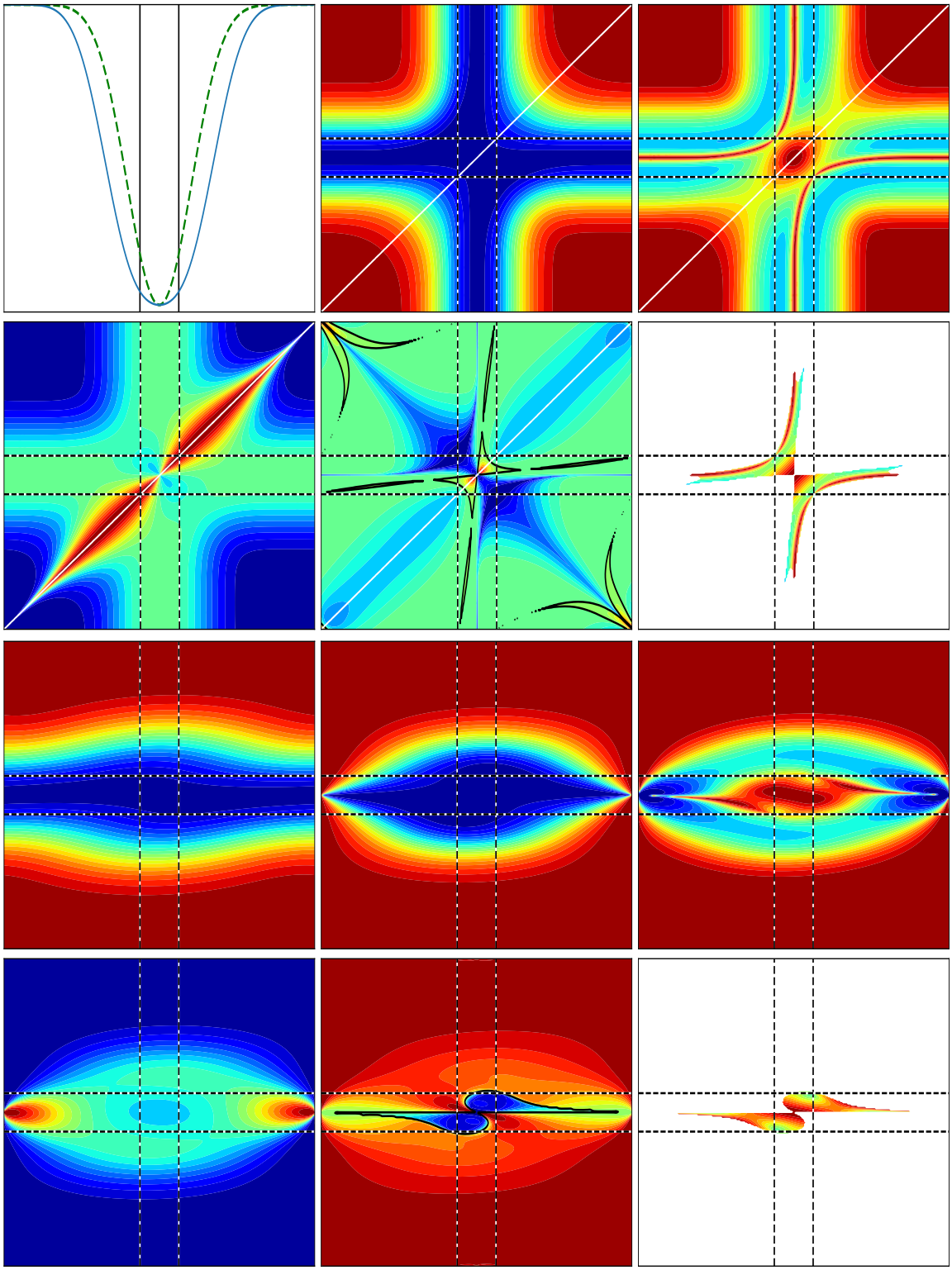

SM6.2. $(d, z, \phi, \lambda) = (6, 1/2, \pi/8, 0)$.

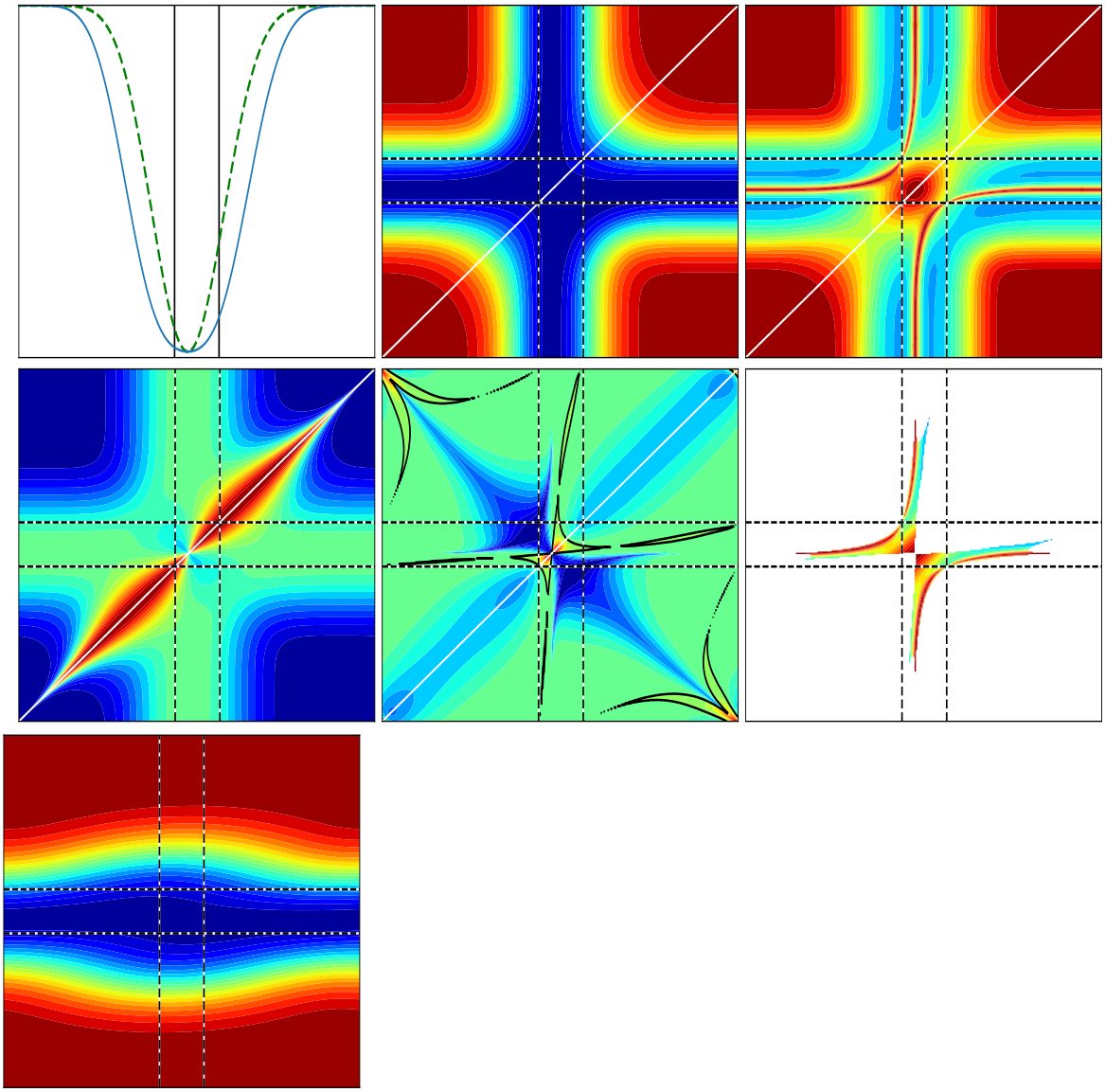

SM6.3. $(d, z, \phi, \lambda) = (6, 0, \pi/8, 0)$.

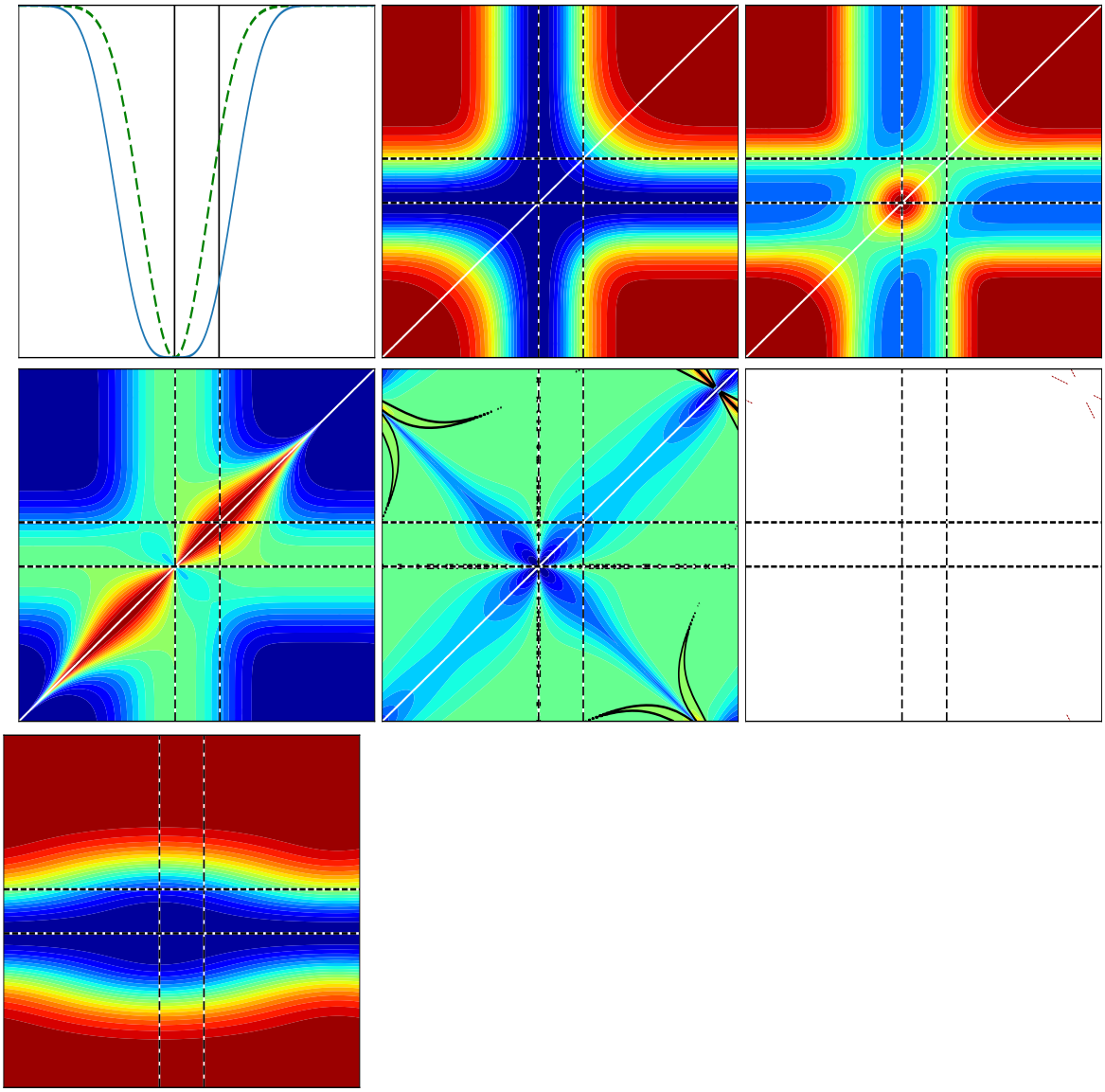

SM6.4. $(d, z, \phi, \lambda) = (6, -1/2, \pi/8, 0)$.

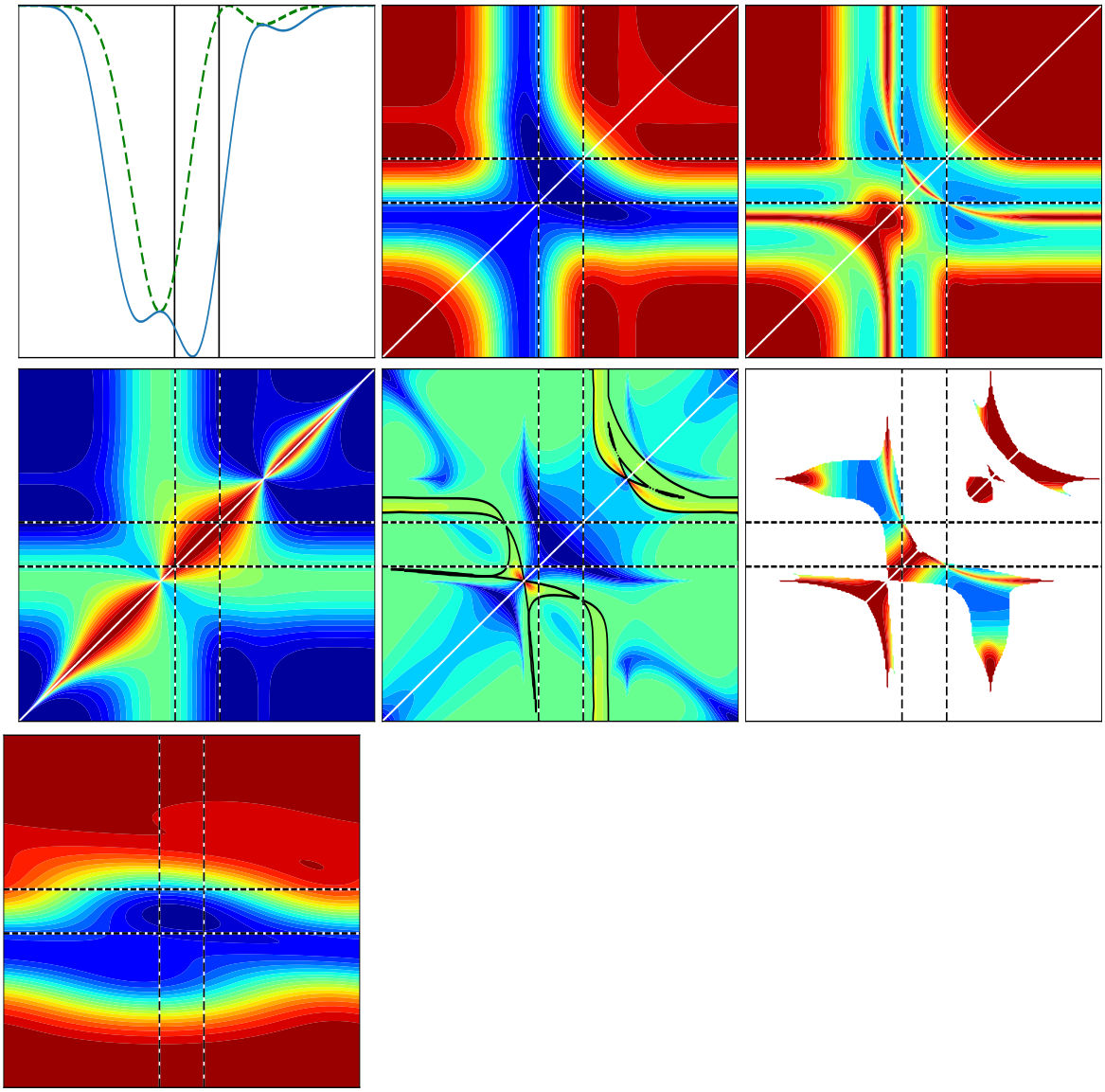

SM6.5. $(d, z, \phi, \lambda) = (6, -1, \pi/8, 0)$.

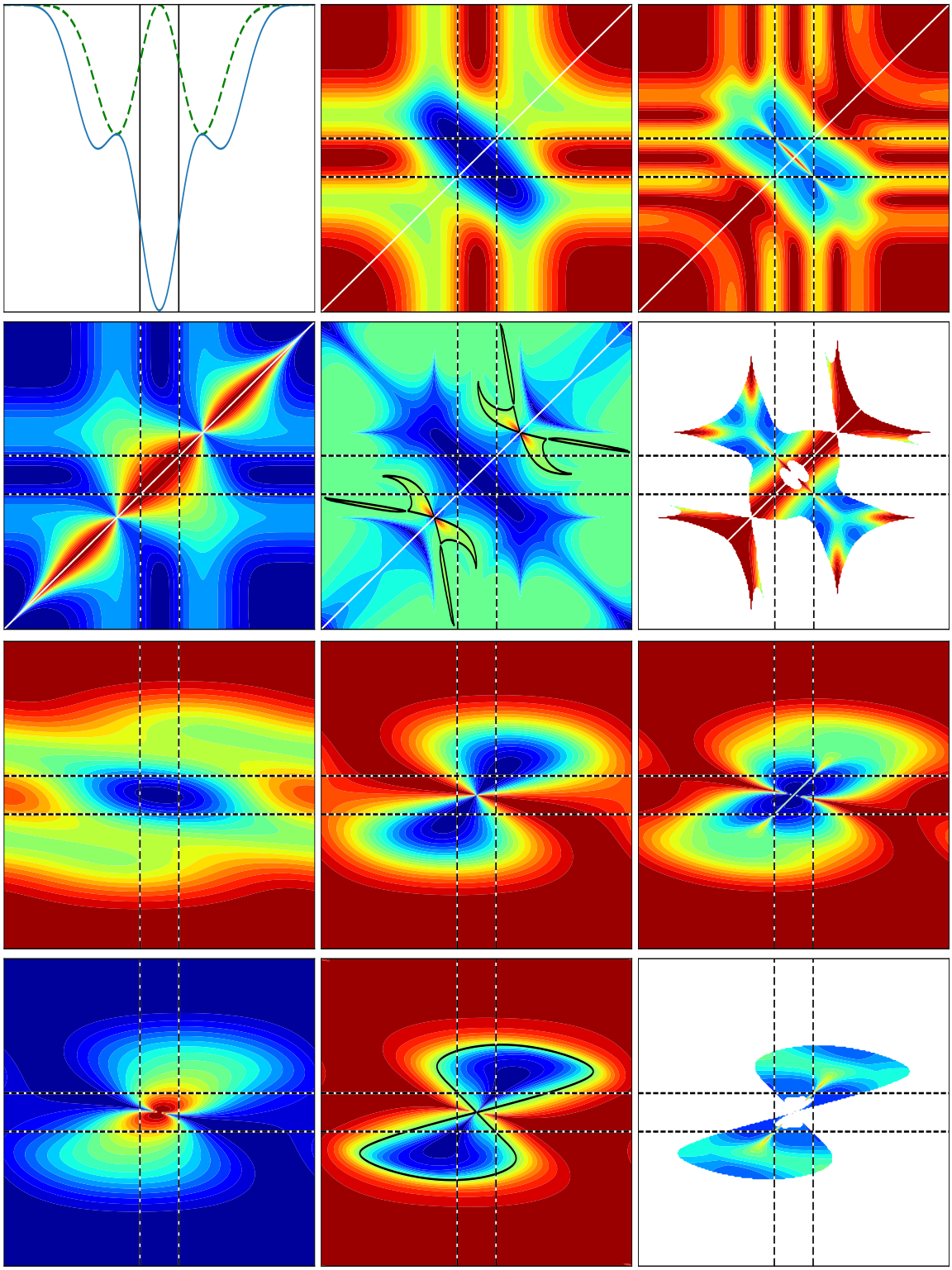

SM7. Varying λ with $(d, z, \phi) = (6, 1, \pi/8)$. The following pages show λ values 0, 1/100, and 1/10.

- For $\lambda > 0$, the vicinity around the minimum shows large algorithm time, but this is not significant since the minimum error is strictly greater than zero.
- For $\lambda > 0$, the discontinuities and essential saddles are removed.
- For $\lambda > 0$, strips of instability with respect to the symmetric set have developed near the diagonal. Around these, strips of stability with respect to the gradient flow have developed, which may slow algorithms.
- For $\lambda = 1/100$, the effects are short range, near $\boldsymbol{\alpha} = \boldsymbol{\beta}$.

SM7.1. $(d, z, \phi, \lambda) = (6, 1, \pi/8, 0)$.

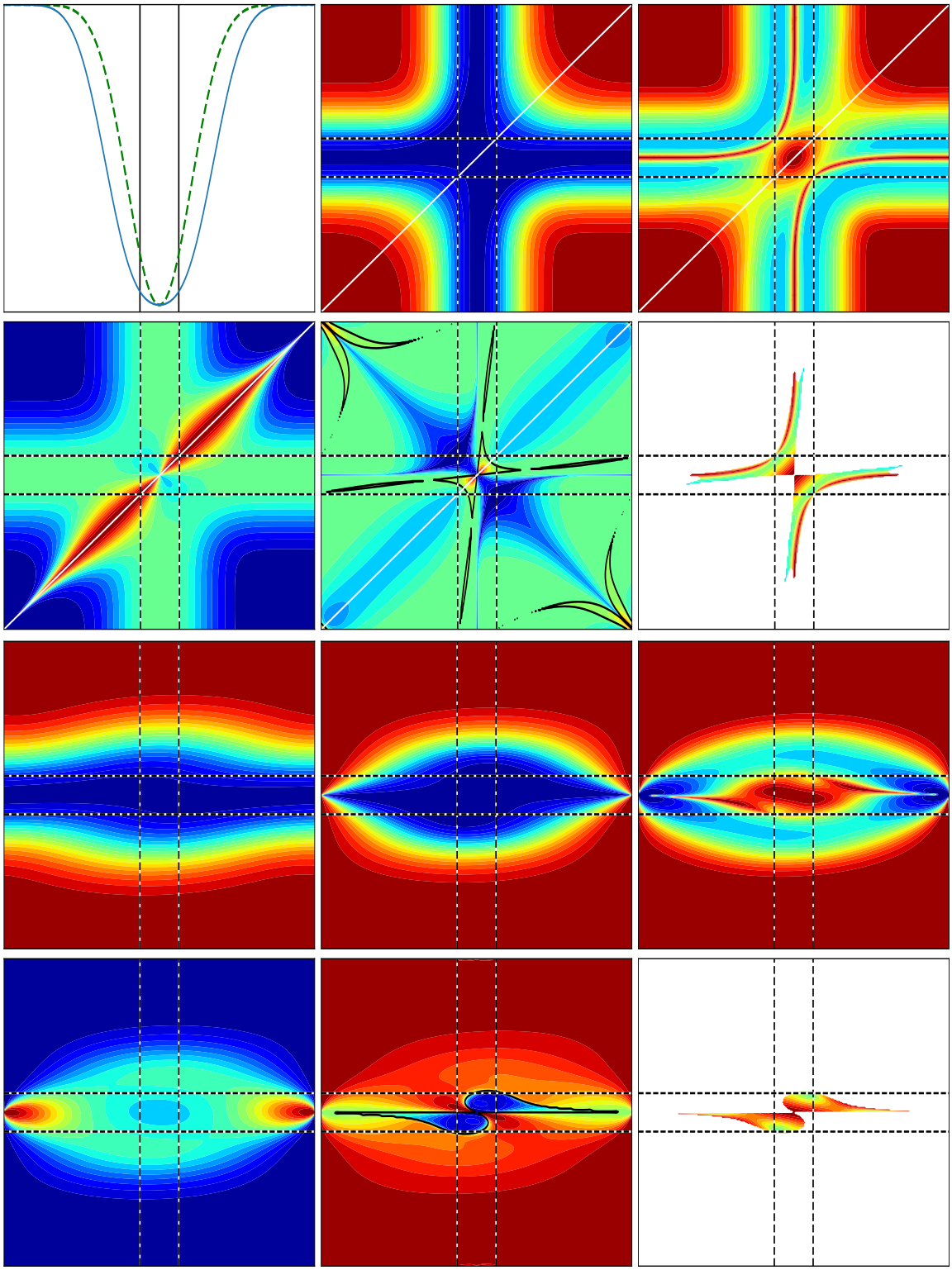

SM7.2. $(d, z, \phi, \lambda) = (6, 1, \pi/8, 1/100)$.

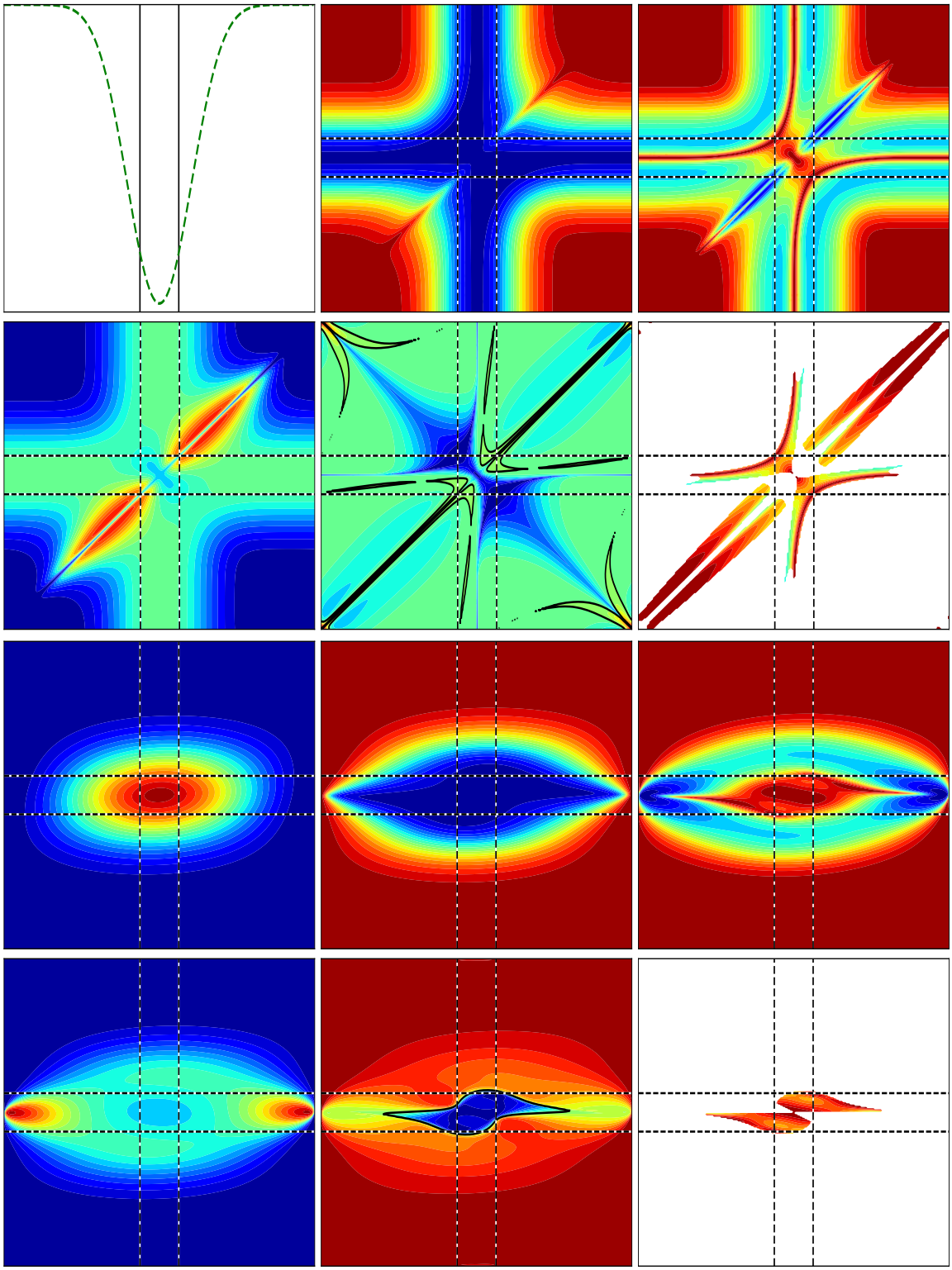

SM7.3. $(d, z, \phi, \lambda) = (6, 1, \pi/8, 1/10)$.

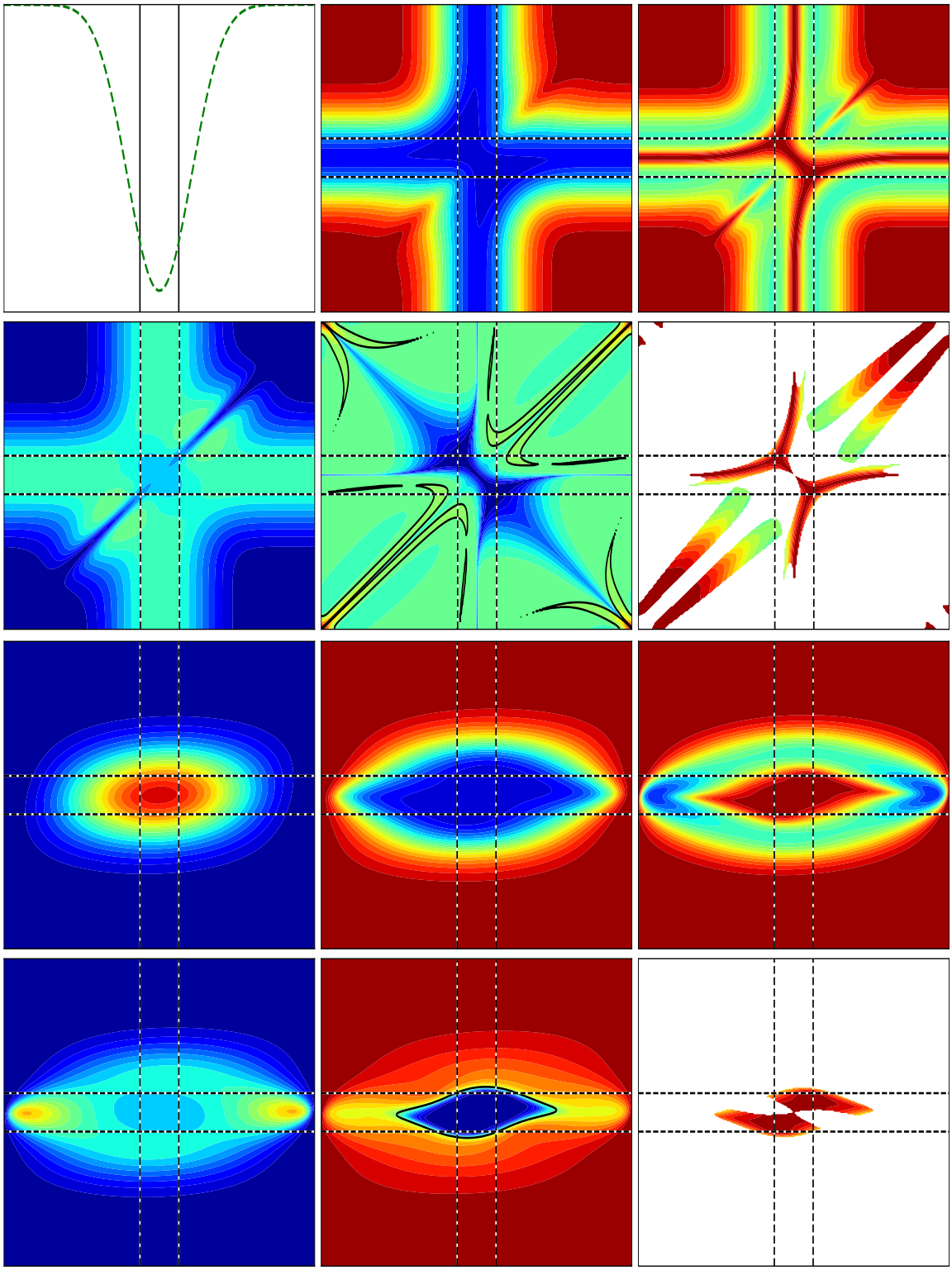

SM8. Varying λ with $(d, z, \phi) = (6, -1, \pi/8)$. The following pages show λ values 0, 1/100, and 1/10.

- The amplitude, error, and stability transverse to the symmetric set change similarly to the $z = 1$ case in section SM7.
- The local infima along the diagonal $\alpha = \beta$ persist as local minima. However, the flow is now unstable in the transverse direction at this point, indicating that they are now saddles in the full parameter space.

SM8.1. $(d, z, \phi, \lambda) = (6, -1, \pi/8, 0)$.

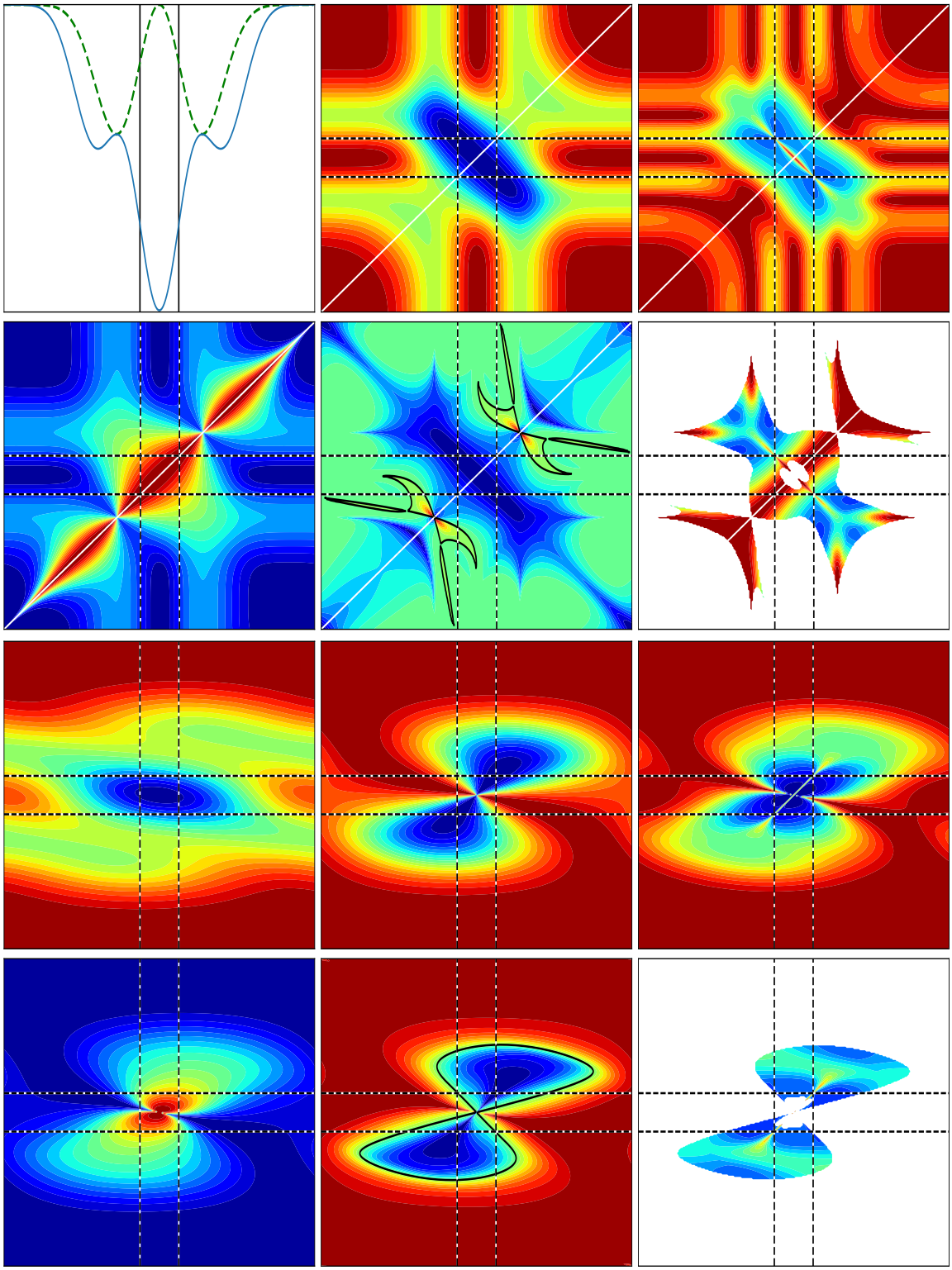

SM8.2. $(d, z, \phi, \lambda) = (6, -1, \pi/8, 1/100)$.

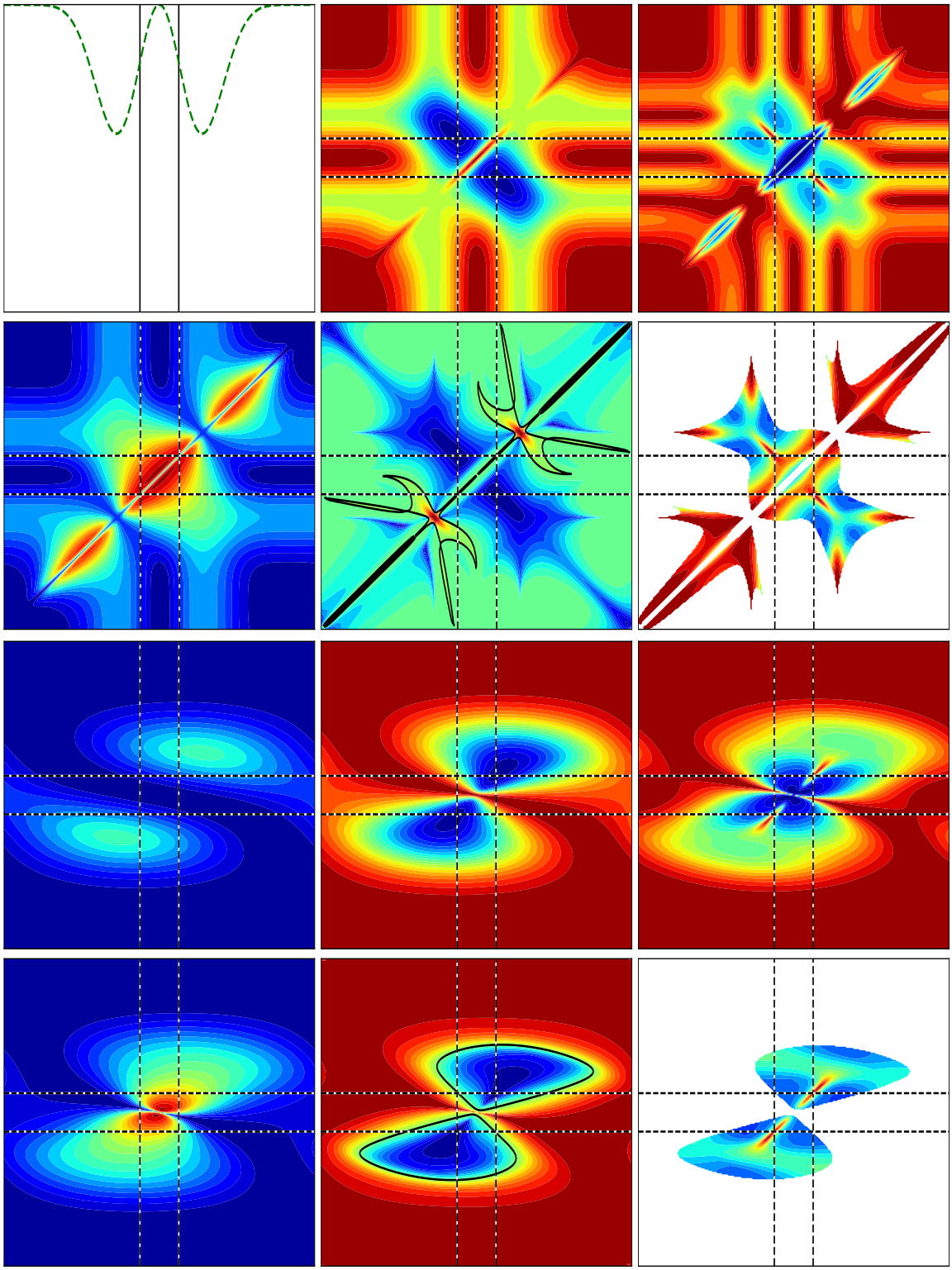

REFERENCES

[1] X. Gong, M. J. Mohlenkamp, and T. R. Young, *The optimization landscape for fitting a rank-2 tensor with a rank-1 tensor*, SIAM J. Appl. Dyn. Syst., 17 (2018), pp. 1432–1477, https://doi.org/10.1137/17M112213X.